Particulate Matter Emissions from a DISI Engine under Cold-Fast-Idle Conditions for Ethanol-Gasoline Blends

by
Iason Dimou

B.S., Naval Engineering,
Hellenic Naval Academy, 2001

Submitted to the Department of Mechanical Engineering in Partial Fulfillment of the Requirements for the Degrees of

MASTER OF SCIENCE IN MECHANICAL ENGINEERING
and
NAVAL ENGINEER
at the
MASSACHUSETTS INSTITUTE OF TECHNOLOGY

May 2011
[June 2011]

Signature of the author: .....
Department of Mechanical Engineering
May 10, 2011

Certified by: .....
Wai K. Cheng
Professor of Mechanical Engineering, Thesis Supervisor

Certified by: .....
Raymond Scott McCord
Senior Lecturer of Mechanical Engineering, Thesis Reader

Accepted by: .....
David Hardt
Chairman, Department Committee on Graduate Students

Particulate Matter Emissions from a DISI Engine under Cold-Fast-Idle Conditions for Ethanol-Gasoline Blends

by

Iason Dimou

Submitted to the Department of Mechanical Engineering on May 12, 2011,
in partial fulfillment of the requirements for the degrees of
Master of Science in Mechanical Engineering and Naval Engineer

Abstract

In an effort to build internal combustion engines with both reduced brake-specific fuel consumption and better emission control, engineers developed the Direct Injection Spark Ignition (DISI) engine. DISI engines combine the specific higher output of the spark ignition engine, with the better efficiency of the compression ignition engine at part load. Despite their benefits, DISI engines still suffer from high hydrocarbon, NO_x and particulate matter (PM) emissions. Until recently, PM emissions have received relatively little attention, despite their severe effects on human health, related mostly to their size. Previous research indicates that almost 80% of the PM is emitted during the first few minutes of the engine's operation (cold-start-fast-idling period). A proposed solution for PM emission reduction is the use of fuel blends with ethanol.

The present research experimentally measures the effect of ethanol content in fuel on PM formation in the combustion chamber of a DISI engine during the cold-start period. A novel sampling system has been designed and combined with a Scanning Mobility Particle Sizer (SMPS) system, in order to measure the particulate matter number (PN) concentration 15 cm downstream from the exhaust valves of a DISI engine, for a temperature range between 0 and 40°C, under low load operation. Seven gasohol fuels have been tested with the ethanol content varying from 0% (E0) up to 85% (E85). For E10 to E85, PN modestly increases when the engine coolant temperature (ECT) is lowered. The PN distributions, however, are insensitive to the ethanol content of the fuel. The total PN for E0 is substantially higher than for the gasohol fuels, at ECT below 20°C. However, for ECT higher than 20°C, the total PN values (obtained from integrating the PN distribution from 15 to 350 nm) are approximately the same for all fuels. This sharp change in PN from E0 to E10 is confirmed by running the tests with E2.5 and E5; the midpoint of the transition occurs at approximately E5. Because the fuels' evaporating properties do not change substantially from E0 to E10, the significant change in PN is attributed to the particulate matter formation chemistry.

Thesis Supervisor: Wai K. Cheng
Title: Professor of Mechanical Engineering

Acknowledgments

A number of people have contributed to making my time at MIT a memorable, always interesting, and extremely rewarding experience. My time at the Institute has afforded me a multitude of opportunities to grow and develop on a number of levels, and for that I am extremely grateful.

Firstly, I would like to thank my advisor, Professor Wai K. Cheng. Since the day he gave me the opportunity to work in his research team, he stood by me and guided me throughout my scientific journey. I learned a lot from him, both in the lab and in the classroom, and due to him I became a better scientist, engineer and researcher.

Also, I would like to thank Dr. Kenneth Kar, who helped me and guided me through my project; he was always there to answer all my questions and advise me. The last few years, I had the privilege to cooperate with excellent students and researchers, working in MIT Sloan Automotive Laboratory as well, to whom I would like to express my gratitude: Emmanuel Kasseris, Kevin Cedrone, Dr. Alex Sappok, Eric Senzer; they all were there to advise, help and support me, when I need it. I would be remiss if I did not acknowledge the Sloan Automotive Lab staff: Thane DeWitt and Raymond Phan for their significant contribution to my project.

For sponsoring my graduate studies I would like to thank the Hellenic Navy.

On a personal level, I wish to express my gratitude to Raymond Scott McCord, Captain (Ret.) USN and Senior Lecturer at MIT, not only for reading my thesis but also because he inspire me to choose internal combustion engines as a research field here at MIT. Finally, I would like to thank Professor Elias Yfantis (Hellenic Naval Academy), for his continuous mentoring and support throughout my work.

Most of all, I would like to thank the person without which none of the above would have been possible: my wife Anna Pakiou. Her encouragement, her inspiration and her unconditional love kept me going all the way. The days and evenings that I was working in the lab, she kept our family together and took care of our two children, Giorgos and Eleni.

Contents

List of Figures

List of Tables

Chapter 1

An Introduction to DISI Engines and Particulate Matter Emissions

This chapter serves two main purposes: firstly, it provides the necessary background information for readers who are not familiar with the concept of Direct Injection Spark Ignition (DISI) engines or the importance of reducing the emitted Particulate Matter (PM) emissions from the modern Internal Combustion Engines (ICEs) in general. Secondly, this chapter describes the specific hypothesis tested by this experimental research approach. This hypothesis addresses the issue of what would be the impact of increasing the ethanol content of fuel on PM emissions from a modern DISI engine and, as a result, on human health. The methodology and the conclusions to this issue will be addressed in subsequent chapters.

1.1 DISI Engines Fundamentals

Since their first appearance in the late 1800s, reciprocating Internal Combustion Engines (ICEs) served humanity in several ways, mainly for transportation and for energy generation. Since then, the constant effort of engineers has improved the performance of ICEs substantially, but their use continues to have a negative impact on the environment. Thus, the challenge for ICE manufacturers remains the same: to develop engines that provide both reduced brake-specific fuel consumption (BSFC) and better emission control. Researchers, over the last decades, developed an ICE that takes advantage of the best features of spark ignition (or gasoline) and compression ignition (or diesel) engines, while suppressing the dis-

advantages of both. The result of this research, the *Direct Injection Spark Ignition (DISI) engine*, combines the specific higher output power of the spark ignition engine with the better efficiency of the compression engine at part load. The DISI engine exhibits a BSFC approaching that of a diesel engine while maintaining the operating characteristics of a gasoline engine [25].

The DISI concept is a variation of conventional SI technology, the fundamental difference being the mixture preparation strategy. For all ICEs, the mixture formation mechanism of air and fuel defines the quality of combustion, which determines the conversion of heat into work and its effects, in terms of BSFC and exhaust gas composition. In spark ignition engines, the initiation of chemical reactions is provoked by the spark plug, and their propagation (flame front) requires similar chemical and thermal conditions in any direction. The more homogeneous the mixture is, the more efficient the combustion process [23]. Prior to the development of the DISI approach, the simpler solution to achieve this was to introduce an already-prepared mixture into the combustion chamber by injecting the fuel into the ports in the cylinder head or into the inlet manifold, allowing enough time for mixture with the air (carburetor system or manifold injection strategy - Figure 1.1). The fuel injection in the manifold close to the intake valves (or Port-Fuel Injection - PFI) during the air intake phase has some advantages, most important of which is the sufficient time allowed for homogeneous mixture formation; however, there are some significant drawbacks. For example,

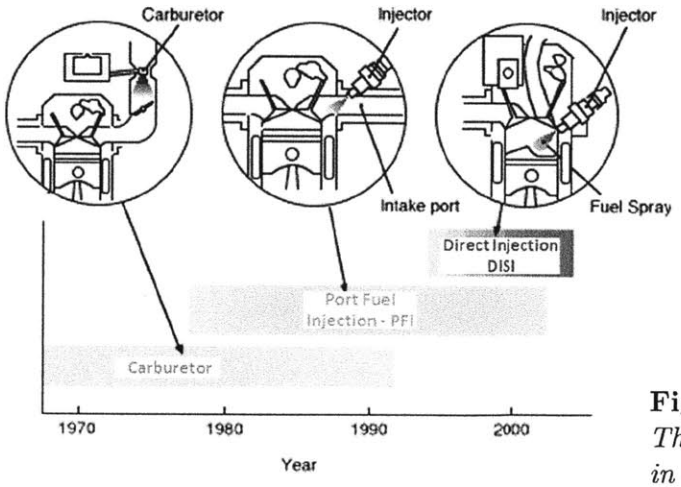

Figure 1.1
The air-fuel mixture formation techniques in spark ignition engines the last 50 years.

in PFI engines, during cranking and cold starting, a transient film of liquid fuel is formed in the intake valve of the port, which cannot be accurately metered - resulting in unstable combustion during the first 5-10 cycles of operation and higher engine-out emissions of un-

burned hydrocarbons [6]. Another limitation of PFI engines is their requirement to throttle the inducted air for basic load control, which leads to thermodynamic losses associated with the negative pumping loop and thus to thermal efficiency degradation, particularly at low levels of engine loads. The DISI engine can operate at very lean overall equivalence ratio by stratification so that the pumping losses can be reduced substantially.

Applying the diesel injection strategy of injecting the fuel directly into the cylinder, while maintaining the ignition spark, the DISI engine has the following advantages:

a. Precise fuel metering into the cylinder. Accurate control of the fuel mass entering the cylinder gives DISI engines the potential for leaner combustion and thus less CO_2 emissions, less cylinder-to-cylinder and cycle-to-cycle variations in the air/fuel ratio and reduced BSFC. Also, control of the engine's load through fueling rate adjustment, when operating lean, reduces the throttling losses. In their comparison, Alkidas and Tahry [1] conclude that the tested DISI engine economizes by 15% on fuel compared to a PFI engine. The biggest positive contributor to this is the reduced pumping losses, which account for a 10% gain in fuel consumption. Spicher et al. [22] showed an even higher reduction of 58% in fuel consumption for a single cylinder engine tested, using both DI and PFI strategies.

b. Charge cooling effect. With the introduction of the liquid fuel in the combustion chamber during the intake phase, the fuel droplets evaporate, absorbing heat from the residual gases and from the fresh charge. Thus the temperature of the mixture is reduced. The charge cooling by the latent heat of vaporization leads to better volumetric efficiency and lower heat losses. Also, the reduction of the mixture temperature at the time of ignition allows higher compression ratio operation, which improves the knocking margin and the thermodynamic cycle efficiency [3, 12].

DISI engines may be classified into three types, according to the mechanism which dominates the mixture formation: wall-guided, air-guided or spray-guided (Figure 1.2). In the first two categories the injector is placed away from the spark plug in the cylinder head and the injected fuel spray is directed towards the spark plug by spray diversion at the piston surface (wall-guided) or by a well-defined in-cylinder air motion (air-guided). In the spray-guided combustion system, the close arrangement of the injector and the spark plug provides a strong coupling between the fuel preparation and ignition (the mixture preparation is dominated by the spray dynamics itself) [17, 10, 20]. Recent research shows that the last system provides higher fuel economy and less emissions compared with the first two [24, 18, 19, 2].

For the automobile industry, the main motivation towards DISI engines comes largely from

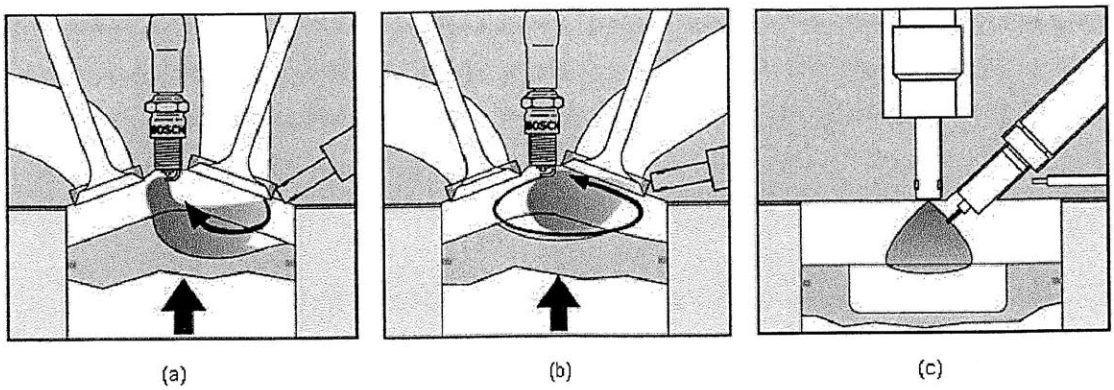

Figure 1.2. *DISI Engines are classified based on the dominated mixture formation mechanism into three categories: a. wall-guided, b. air-guided and c. spray-guided [17].*

their potential for lower fuel consumption and CO_2 emissions compared to PFI gasoline engines. Despite these benefits, DISI engines still suffer from high Hydrocarbon, NO_x and Particulate Matter emissions. For example, Cole R. et al. [7] measured 2.9 times higher Total Hydrocarbon (THC) and 9.5 times higher NO_x emissions between a 1998 DISI engine and a 1995 PFI engine (in the same paper the DISI engine had a 24% better fuel economy). A more recent comparison between several types of ICEs from modern vehicles is presented by Braisher M. et al. [5]. Diesel engines without Diesel Particulate Filter (DPF) systems and DISI engines emit more than the current EU regulations for both PM mass and PM number concentrations (Figure 1.3). HCs emissions from gasoline engines are reasonably well documented in the literature. Until recently, PM emissions from DISI engines have received relatively little attention, despite their severe effects on human health (PM from gasoline cars are still not legislated in the USA). The next section presents the necessary background for the PM formation mechanisms and emissions from ICEs and their effects on human health, and explain in more detail the PM sources in DISI engines.

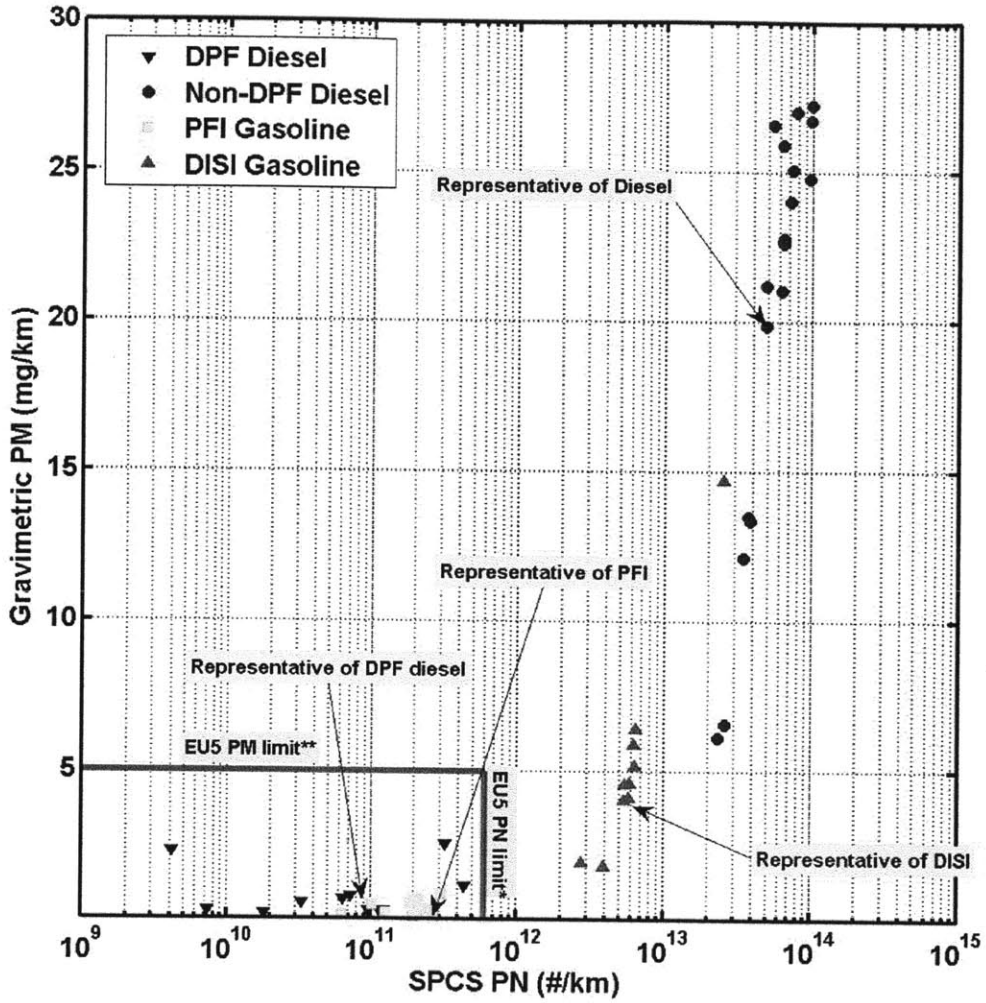

Figure 1.3. *A comparison between modern vehicles under the new European drive cycle (NEDC) shows that diesel engines without DPF technologies and DISI engines emit an order of magnitude more particulate matter in both number (horizontal axis - PN) and mass (vertical axis - PM) than the PFI gasoline engines. These values exceed the legislated European limits [5].*

1.2 Particulate Matter Emissions from Internal Combustion Engines

In the context of Internal Combustion Engines' emissions, Particulate Matter (PM) is the term used for the solid and liquid droplets suspended in exhaust products. Historically, PM emissions have been associated with diesel engines because PM produced by diffusion combustion exceeds by far the PM produced by a premixed charge (gasoline engines). That is not the case for DISI engines. Their PM emissions are closer to that of diesels and thus, the gained experience from research in this field is applicable here as well. The PM produced by modern ICEs is mostly carbonaceous, organic or sulfurous, with individual particles ranging in size from a few nanometers to a few micrometers (Figure 1.4). According to many epidemiological studies, PM is the most severe pollutant in terms of adverse effects on human health, mostly as a function of particles' size. Due to the increase of DISI engines' production, globally, governments around the world are currently discussing the limits needed to be imposed for PM emissions from DISI engines in both mass and number concentration. The following paragraphs present a brief introduction to these issues.

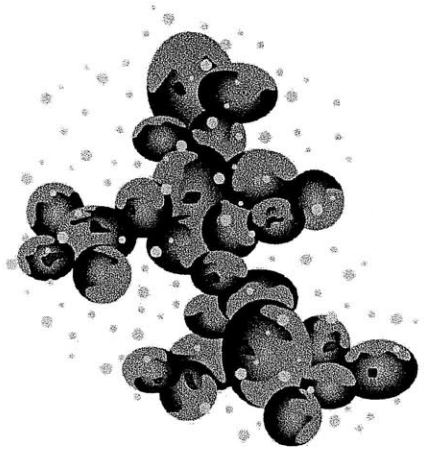

Figure 1.4
Artist's Conception of PM: PM are formed from elemental Carbon (black), Inorganic Material (blue) and other volatiles (yellow) that may stick on the PM surface. All these form agglomerates with a range from 20 to 2500 nm.

1.2.1 PM Formation and Chemical Composition

PM has different chemical composition, depending on its sources. Macroscopically, the main sources of PM are the fuel and the lubricating oil, but different chemical processes may result in different PM compositions. Engine fuels are typically mixtures of many different hydrocarbons (alkanes, cyclo-alkanes, olefines, aromatics, etc). In addition, several sulphurous, inorganic and organometallic compounds may also be present. These may be either residual

material from the crude oil (part of an additive pack), or contamination. Engine lubricating oils predominantly consist of hydrocarbon compounds. However, lower levels of other material are also present.

In a combustion chamber, typically, 99% of the hydrocarbons will be oxidized during the combustion process. The unburned hydrocarbons and the inorganic material, which will be carried through the combustion process, appear as PM in the exhaust gases (Figure 1.5).

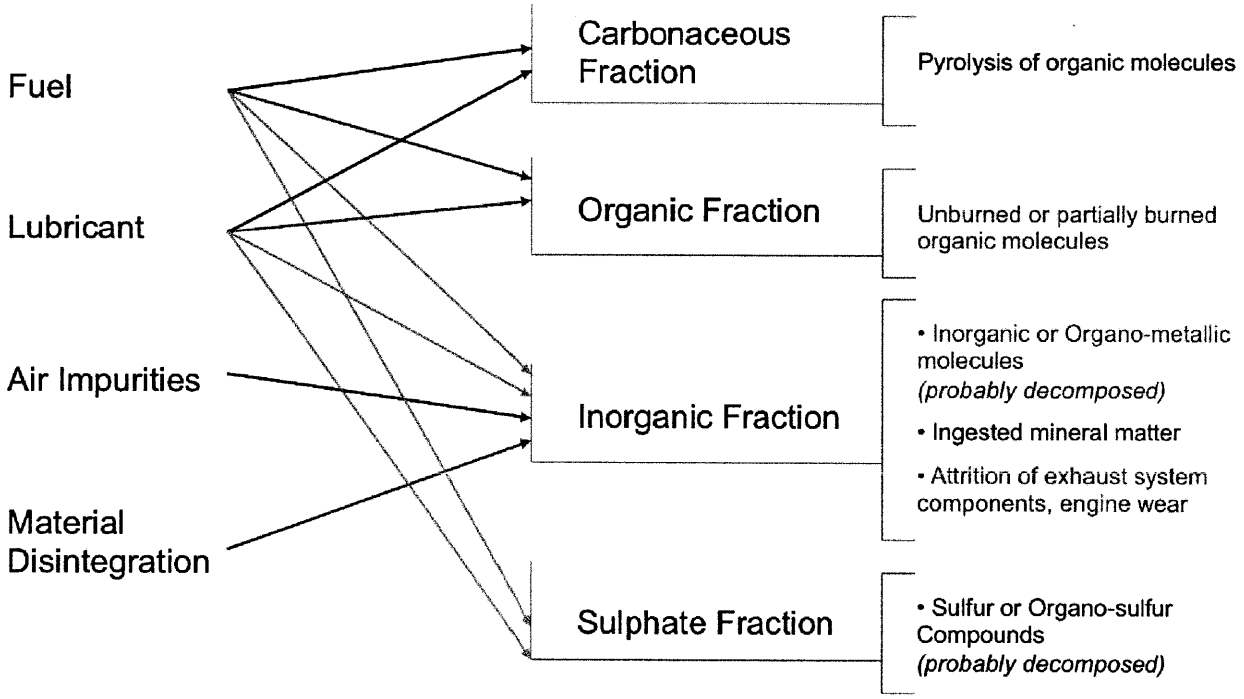

Figure 1.5. *The emitted PM are formed mainly from the unburned hydrocarbons of fuel and oil and from the inorganic material that was carried through the combustion [8].*

1. The Elemental Carbon Fraction

According to the laws of thermodynamics, pyrolytic soot formation begins in rich combustion environments or even under stoichiometric or lean conditions in locally rich zones, when fuel films are deposited on surfaces, or due to charge heterogeneity (incomplete mixture of the fuel with the air or incomplete evaporation of fuel droplets).

The process of PM formation is still not completely understood, because it is happening with many parallel and fast reactions, i.e. the time of conversion of methane with a molecular weight of 16 amu to soot particles with a molecular weight of 10^6 amu is 10^{-4} - 10^{-2} sec [15].

PM starts with the formation of Polycyclic Aromatic Hydrocarbons (PAH) and unsaturated hydrocarbons (HC) at locally rich areas of combustion during the pyrolysis of the fuel. PAHs are important precursors (nuclei) of soot particles with a molecular weight of 500-2000 amu. The further particle growth is due to the surface growth in reactions involving many acetylene molecules (Figures 1.7 and 1.8), in parallel with particle to particle collisions (coagulation), where coalescence leads to fractal agglomerates of primary particles. By the time particles are emitted from the cylinder of an engine, agglomerate sizes may be of the order of 100 nm.

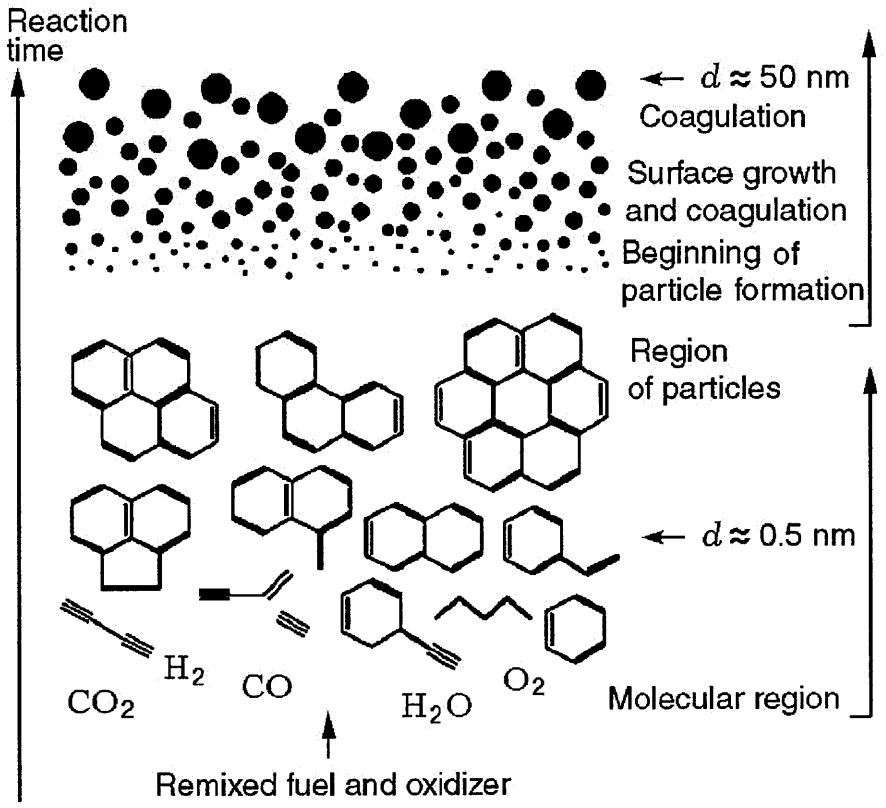

Figure 1.6. *Rich fuel areas of the combustion chamber has as result the formation of PAHs, which serve as precursors of soot particles. These nuclei grow by several mechanisms (coagulation, order to form larger PM [15].*

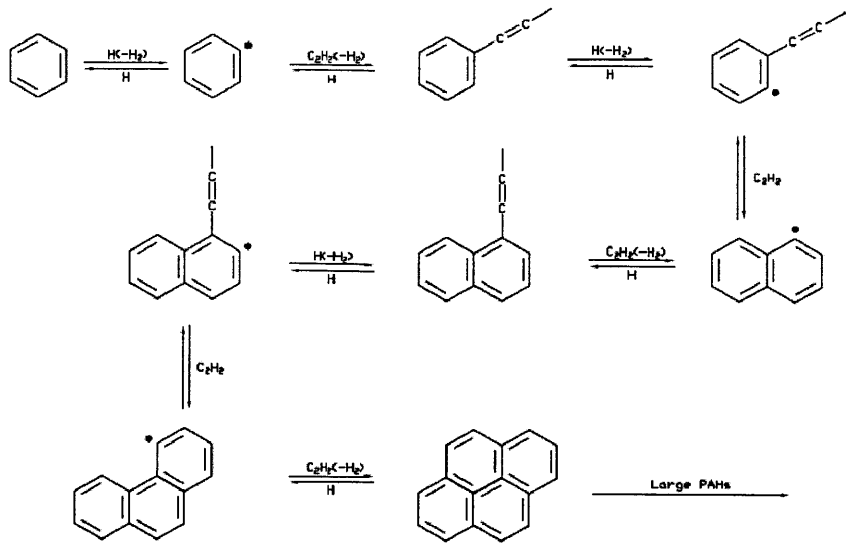

Figure 1.7. *The H-Abstraction-C2H2-Addition (HACA) mechanism of Polycyclic Aromatic Hydrocarbon (PAH) formation [20].*

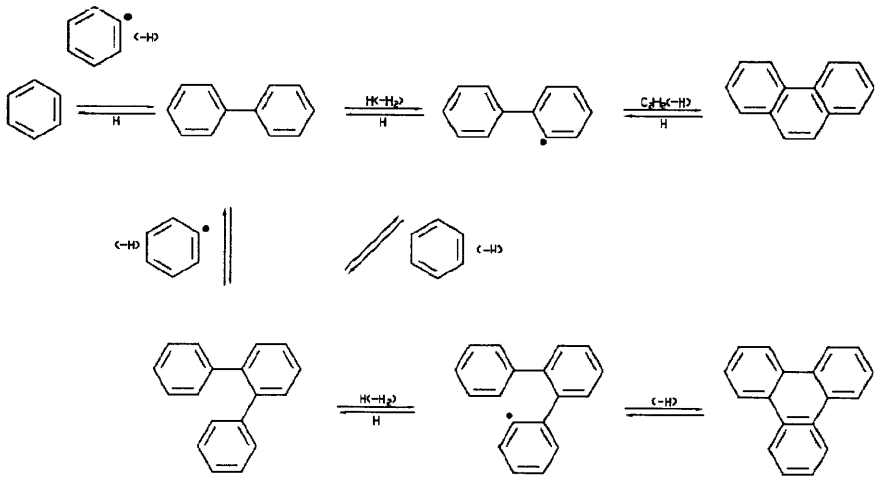

Figure 1.8. *An alternative mechanism of PAH growth [20].*

2. The Volatile Organic Fraction

The Volatile Organic Fraction (VOF) of the PM describes the fraction of the PM that exists in the liquid phase, either as dispersed liquid droplets, or adsorbed onto the surface of soot agglomerates. VOF includes compounds found in the fuel and lubricant, which are carried

through the cylinder unchanged, or VOF can include new species not present in the fuel (or in the lubricant), synthesized from interrupted pyrolytic reactions. However it is difficult to distinguish the PM fractions that come from the fuel vs those derived from the lubricant. Generally, the organic material existing as VOF is less volatile (higher molecular weight) than that which exists as gas phase HC. There is also often a correlation between HC and VOF emissions since some of the conditions leading to each are similar.

3. The Inorganic Fraction

The inorganic fraction consists of several different inorganic materials, such as Calcium, Magnesium, Zinc, Iron, etc, that may be present in the PM. Similar to volatile organic material, inorganic material is found both adsorbed to the surface of soot agglomerates, and also existing as a nucleation mode. The main sources for the inorganic material are the additive packages in the fuel (such as Ferrocene and MMT) and lubricant (such as Zinc-Dialkyl-Dithio-Phosphate). In addition to fuel and lubricant additives, inorganic material such as mineral dust can be ingested with the intake air-stream, pass through the cylinder and contribute to the emitted PM. Finally, inorganic material may also derive from wear of the base engine.

4. The Sulphate Fraction

The Sulphate fraction describes the fraction of the particulate containing sulphate particles, which could exist either as particles in a nucleation mode, or adsorbed to the surface of larger soot aggregates. The Sulphur in question derives from the fuel and lubricant, which in turn derives from crude oil. Although regulations demand ultra-low sulfur fuels, some sulfur remains in such fuels and this provides a source of Sulphur that contributes to a sulphurous fraction in the PM. Particulate phase sulphuric acid or sulphate is undesirable because it adversely affects exhaust after-treatment systems by deactivation of catalytic surfaces. It is also undesirable in the atmosphere due to acid rain and the albedo effect.

1.2.2 Aerosol dynamics and PM sampling challenges

Particles have irregular and anisodiametric morphology. From an analytical point of view, it is convenient to ignore their shape irregularities; thus the concept of *equivalent diameter* (=diameter of a sphere with the same value of a physical property as that of the irregular particle) is usually used when PN distributions are presented. There are several types

of equivalent diameters, based on the sampling process: aerodynamic diameter, Stokes' diameter, Feret's diameter, and others [11]. An instrumentation frequently used within the industry and laboratories globally is the Scanning Mobility Particle Sizer (SMPS). SMPS counts the particles within a predefined range (few nm up to 1 μm) and plots them based on their electrical mobility diameter (=the diameter of a sphere with the same electrical mobility as the particle).

For different particle sizes, the number concentration may vary several orders of magnitude. Thus it has become common to describe the PN distribution in terms of the logarithm of particle size, or $dN/dlogd_p$, where N is the particle number concentration and $dlogd_p$ is the differential interval of the logarithm of particle size. Although there is no obvious theoretical basis for particle size distributions, available empirical data fits well with a lognormal distribution:

$$\frac{dN}{dlogd_p} = \frac{N}{\sqrt{2\pi}log\sigma_g} \cdot exp\left[\frac{(logd_p - logCMD)^2}{2(log\sigma_g)^2}\right], \tag{1.1}$$

where

$$\sigma_g = exp\left(\frac{\int_0^\infty (logd_p - logCMD)^2\, dn}{N-1}\right)^{1/2}, \tag{1.2}$$

CMD is the Count (number) Median Diameter,
σ_g is the geometric standard deviation and
n is the number of particles.

The distribution of particles from engines exhaust gases are often bi- or tri-modal lognormal distributions (Figure 1.9). Without these being solid boundaries, particles can be characterized based on the size spectra, as:

Nucleation mode	$5 < d_p < 50nm$
Accumulation mode	$50 < d_p < 500nm$
Coarse mode	$d_p > 500nm$

Generally, the PN found in the coarse mode ($d_p > 2.5\mu$m) are low enough to be considered negligible. Given their significant effects on human health, this research focuses more on PN for $d_p < 500nm$ (ultrafine- and nano-particles).

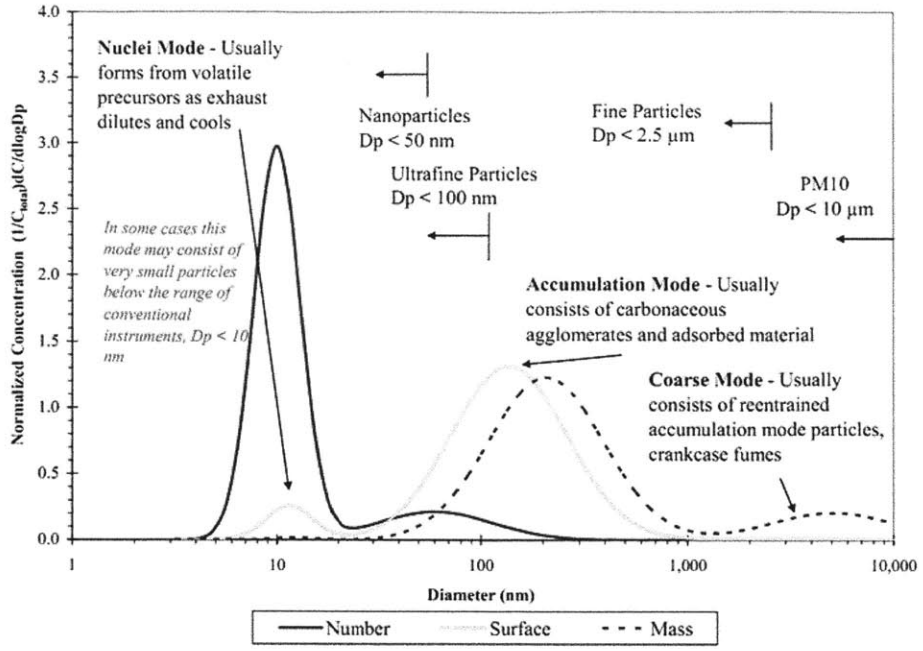

Figure 1.9. *Typical engine exhaust particle size distribution by mass, number and surface area. PN tri-modal lognormal distribution fits well the data from tailpipe engine exhaust gases.*

From the particle size distribution, it is possible to calculate the total PN, within the measured size range with direct integration:

$$N_{total} = \int_{d_{p,min}}^{d_{p,max}} \frac{dN}{dlogd_p} dlogdp \tag{1.3}$$

PN concentrations emitted from ICEs are usually orders of magnitude higher than the maximum range of SMPS or other equivalent instrumentation. Thus, a dilution tunnel is used in order to dilute the exhaust gases from the sampling point, with a particle-free gas. From the mixture, only a small portion goes into SMPS to be analyzed. Due to the dynamic behavior of the particles, it is challenging to ensure that the SMPS does produce the same PN distribution as the sampling point, or to ensure that there are no particle losses during the sampling process. Generally, PN are produced by sampling exhaust gases exiting the tailpipe of the vehicle and diluting them with air in a full dilution tunnel. This research investigates the PM formation in the combustion chamber; thus the sampling point is close to the exhaust valves of the cylinder. In addition, a new sampling system has been designed. Although details of the system are described in Chapter 2, it is important to present a brief introduction to the possible particle loss mechanisms suppressed with our sampling system.

There are two main categories of phenomena that can change the PN distribution during the sampling process: a) some that decreases particle numbers for all sizes due to the collision of particles with wall surfaces, where particles tend to stick (particle losses on the wall), and b) others that alter the particle size. In order to measure the actual PN distribution at the sampling point, these phenomena should be suppressed. The main mechanisms, which can lead to a different PN distribution than the one at the sampling point, are as follows:

a. **Diffusion.** Diffusion, or Brownian Motion, is the irregular wiggling motion of aerosol particles, caused by random variations in the relentless bombardment of gas molecules against them. This random motion causes particle deposition along walls of tubes. Smaller particles can diffuse more quickly and therefore diffusional deposition is most important for these small particles and for small diameter tubes.

b. **Thermophoresis.** Thermophoresis is a phenomenon where in the motion of particles occurs as a result of a temperature gradient. This is especially important when particles are moving in hot gas environments. The particles experience more collisions from the gas molecules in the hotter side, which causes a bulk motion of the particles towards a cooler region, i.e. wall surfaces.

c. **Adsorption/Desorption.** Adsorption is the adherence of species to the particles, while desorption is the release of species from them (opposite mechanism). Specifically, Vapor-phase molecules present in the exhaust can stick to the particles, thus contributing to the overall particle formation and growth. The saturation ratio is the ratio of the partial pressure of the species to the saturation pressure for the same species. Adsorption takes place below the saturation pressure.

d. **Condensation/Evaporation.** Condensation is the transformation of gaseous species to liquid or solid form upon interaction with condensation nuclei, i.e. particles. This takes place above the saturation pressure for a species, continuing until the saturation ratio drops below saturation. At this point evaporation, the opposite of condensation, takes place.

e. **Coagulation.** Coagulation is the process wherein aerosol particles collide with one another, due to a relative motion between them, and adhere to form larger particles. The net result is a continuous decrease in number concentration coupled with an increase in particle size. In the case of solid particles, the process is also called **agglomeration.**

f. **Gravitational Deposition.** Gravitational deposition occurs when particles drop out of

the bulk flow since they are heavier than gas and depends on the time the particles spend in any part of a sampling system. This mechanism does not contribute to particle losses for the particle sizes investigated.

g. **Electrostatic Deposition.** Electrostatic deposition takes place when charged particles are in a path with electrically chargeable walls, like magnetic materials or plastics that can hold a static charge.

All the above phenomena occur simultaneously. A model approach to describe their effects on the PN distribution comes from solving the general dynamic differential equation:

$$\frac{\partial n_k}{\partial t} + \nabla \cdot n_k \overrightarrow{v} = \nabla \cdot D \nabla n_k + \left(\frac{\partial n_k}{\partial t}\right)_{growth} + \left(\frac{\partial n_k}{\partial t}\right)_{coagulation} - \nabla \cdot n_k \overrightarrow{c}, \tag{1.4}$$

where

$$\left(\frac{\partial n_k}{\partial t}\right)_{growth} = -\frac{\partial I}{\partial t} = -\frac{\partial}{\partial t}(-D\frac{\partial n}{\partial v} + n_k \frac{dv}{dt}), \tag{1.5}$$

$$\left(\frac{\partial n_k}{\partial t}\right)_{coagulation} = \frac{1}{2}\int_0^v K(\widetilde{v}, v-\widetilde{v}) \cdot n(\widetilde{v}) \cdot (v-\widetilde{v})\, d\widetilde{v} - \int_0^\infty K(\widetilde{v}, v-\widetilde{v}) \cdot n(\widetilde{v}) \cdot (v-\widetilde{v})\, d\widetilde{v}. \tag{1.6}$$

The left side of the equation shows the time change of the particles and the effect of the particles' transport by convection (gas bulk motion). The right side shows the effect on PN distribution from particle size changes due to a) the concentration gradient (diffusion), b) the particle size growth and coagulation, and c) external fields (gravity, electrical, thermal). In his book [9], Professor Friedlander analyzes all terms of the above equations in more detail. However, this modeling approach is extremely complicated and out of the scope of this research. For the design of our sampling system we identified all possible particle losses and took all possible precautions to avoid them. Experimentally, we optimized the sampling conditions to minimize their effects, which we verified experimentally (Chapter 2).

1.2.3 PM Health Effects and Legislation

According to numerous health studies, particulate matter emissions from ICE cause significant problems to human health, including asthma, lung cancer, cardiovascular disease, and premature death. As an example, in 2009, the estimated number of annual premature deaths related to PM in California is 9,200, with an uncertainty range of 7,300 - 11,000 [4]. The

hazard caused by inhaled particles depends on their chemical composition and on the region of the respiratory system at which they deposit. The extent and the location of particle deposition in the respiratory system depend on a) particle size, density and shape, b) airway geometry, and c) individual breathing patterns. Particles with sizes on the order of 10 μm or less (PM_{10}) can pass through the throat and the nose, and they can reach the lungs. There the particles settle in the bronchi. The 10 μm size does not represent a strict boundary between respirable and non-respirable particles, but most regulatory agencies agree on monitoring airborne particulate matter. Particles smaller than 2.5 micrometers ($PM_{2.5}$) tend to penetrate the gas exchange regions of the lung. Finally, particles with an average diameter less than 100 nm (ultra-fine) may pass through the lungs into the blood stream to affect other organs as well. Pope et. al. [16] indicate that $PM_{2.5}$ leads to high plaque deposits in arteries, causing vascular inflammation and atherosclerosis, which can lead to heart attacks and other cardiovascular problems.

Due to the severe effects of PM emitted from ICEs on human health, governments around the world have legislated limits against them. The PM emission control era began in the early 1970s, with the legislation of smoke from heavy-duty diesels in the USA. The first particulate standards were established in 1980 for passenger cars and light-duty trucks, followed by the heavy-duty engines in 1985. In Europe, PM emissions from engines were first controlled in 1989. Nowadays, PM emissions are strictly regulated in most countries, mainly as emitted PM mass (mg/kilometer). Despite the high PM emissions from DISI engines, these limits apply for most cases only to compression ignition engines, with the exception of EU 5 (effective since 2009) that provides an upper limit of 5 mg/km for DISI engines as well.

PM size is an important determinant as far as PM effects on human health, thus the European Union is currently in the process of imposing an emission limit for total particulate numbers, for both diesel and DISI engines, with a proposed limit of $6 \cdot 10^{11}$ particles/km, for engines manufactured after 2014 (Figure 1.10). The USA does not legislate the PN yet; however it seems that they will draft similar legislations in the near future. In conclusion, PM number concentration from DISI engines will be legislated over the next few years and thus a research effort towards strategizing for PM reduction from DISI engines is necessary.

Currently, in order to measure and compare emissions, vehicles are tested under a series of predefined conditions (driving cycle), including cold start, accelerations, constant speed operations, etc. on chassis dynamometers. These driving cycles represent typical usage of the vehicle. During these runs, exhaust gases exiting the tailpipe of the vehicle are sampled

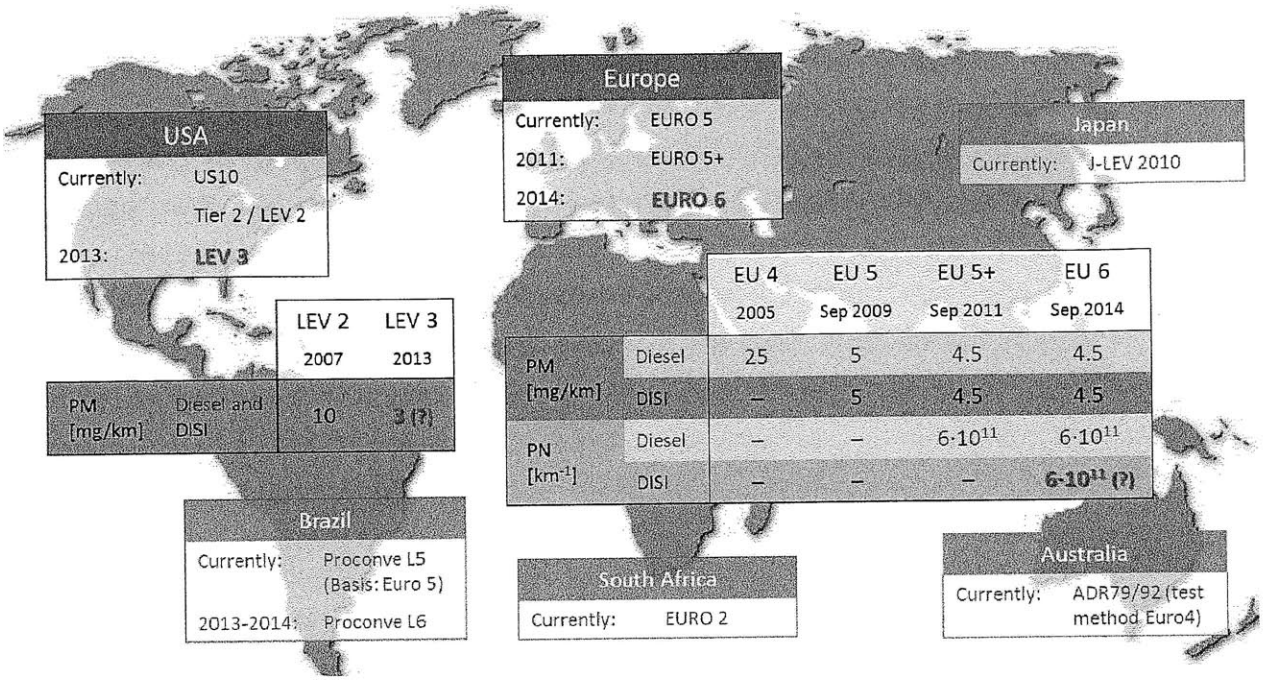

Figure 1.10. *PM emission legislations, for diesel and DISI engines, for countries around the world. In 2011, the EU began legislating not only PM but also PN for diesel engines. In 2014, this legislation will expand to DISI engines as well. Although, the USA has not legislated the PN yet, it is likely they will follow suit over the next few years.*

in order to be analyzed for a variety of hazardous gases, including PM. Figure 1.11 shows an example of PN emissions from a typical vehicle under the New European Driving Cycle, where 80% of the total PN emitted is during the first minutes of engine operation (cold-start period).

During the first minutes of operation, the engine passes through a transient condition: the cylinder walls and the fuel-air mixture are still cold, and the fuel pressure is still low. As a result, the fuel does not evaporate so easy. In addition to that, in order to maintain stable engine operation the ignition timing is late, which increase the injected fuel mass. All these effects increase the probability for incomplete flame operation, wall wetting, locally rich fuel-air charge, crevice storage of the fuel, oil dilution with liquid and fuel vapor, wall quenching, poor post-flame oxidation, etc. A strategy that will reduce the PN emission during this cold-fast-idling period will have significant impact in the reduction of the total PN emission as well. That is the main motivation of this research.

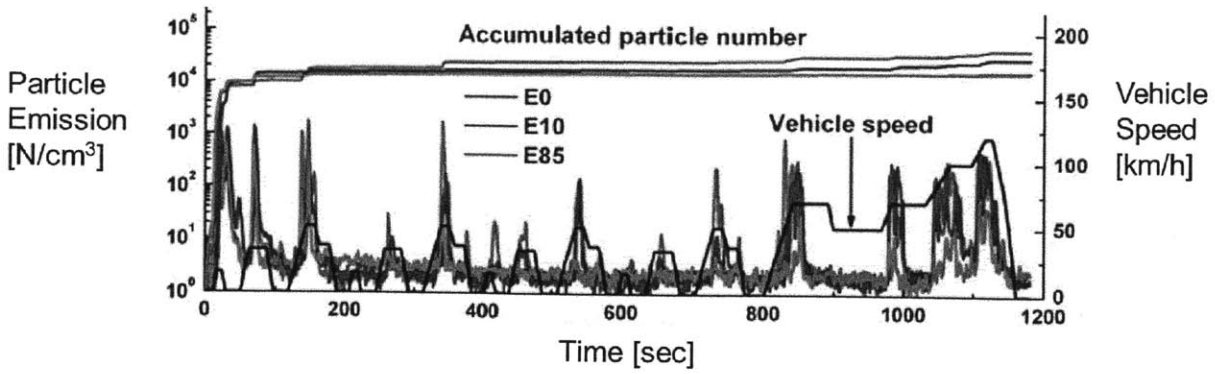

Figure 1.11. *Time-resolved PN concentrations emitted during the New European Driving Cycle for three fuels: E0, E10, and E85 [14].*

1.3 Could Ethanol be a solution ?

Literature provides several examples of research work that targets the reduction of PM emissions from DISI engines, especially in the last few years. In almost all cases the research focused on different in-cylinder strategies (injection duration, split injection, fuel pressure, etc.) to reduce the PM emissions during steady-state warm-up conditions or for the overall driving cycle.

Some authors report the fuel to be the dominant contributor for PM, compared to the other factors reported previously (Figure 1.5), which is not surprising, given that the mass of fuel consumed in one engine cycle is typically two to three orders of magnitude greater than the mass of lubricant consumed. Thus, another approach for PM reduction is the use of alternative fuels.

Gasoline is a mixture of several chemical compounds. Usually 20% of gasoline is aromatic hydrocarbons (henceforth, "aromatics"). As mentioned in a previous section, aromatics, such as benzene, are precursors for PM formation. The presence of ethanol (a fuel with higher oxygenate content in its molecule) in the fuel has a double effect: first, it reduces the percentage of aromatics in the fuel and as a result the potential for PM formation during the pyrolysis and the initial stages of nucleation; also, ethanol contains oxygen atoms (partially oxidized fuel), which may increase the post-combustion oxidation effect, suppressing the PM formation even more.

In addition to the above, ethanol has some advantages over gasoline as a fuel for spark-ignition engines, such as better anti-knock characteristics, and reduced CO and unburned HC emissions. These are some of the reasons that there are several proposals in the USA to increase the amount of ethanol for transportation (passenger cars) and the main motivation of the present research.

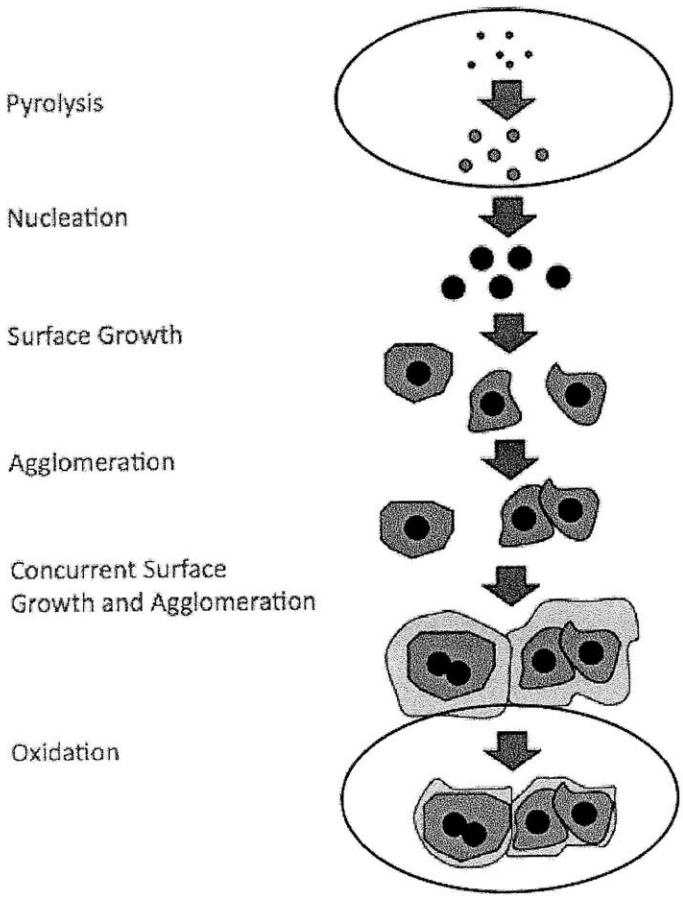

Figure 1.12. *The presence of ethanol target to reduce the aromatic componet of the fuel; thus suppress the PM formation during the pyrolysis and the nucleation phase. The higher oxygenate content of the fuel can increase the oxidation process as well.*

This work investigates the effect of ethanol content in fuel blends of gasoline and ethanol on PM formation in a DISI engine's combustion chamber, during the cold-start-fast-idling operation period. Due to limitations of the instrumentation the transient cold-start period is simulated as a steady-state operation. During the experiments the operating characteristics of the engine were maintained constant. However, the engine temperature varied from 0 to 40°C, to investigate the effect of engine temperature at cold start as well.

Our research effort focuses on the emitted PM number (PN) concentrations in the combustion chamber as a function of particles' size; thus the sampling point for the exhaust gases is only 15 cm downstream from the exhaust valves. A mini-dilution tunnel has been designed to dilute the sample, so that the particle number is within the measurement range of the instrumentation and, at the same time, to minimize the particle losses during sampling. The experimental setup and the methodology are described in Chapter 2. Finally, the results for the different ethanol content levels at each temperature and the conclusions from this work are described in Chapter 3.

Chapter 2

Test Matrix, Experimental Apparatus and Methodology

This chapter describes the methodology followed in this research and the hardware and software used to measure the effect of ethanol on Particulate Matter (PM) formation from a Direct Injection Spark Ignition Engine (DISI) during the cold-start period. First, the experimental matrix is presented, followed by the description of the engine, the PM sampling system and the instrumentation used during our experiments. The goal of this research is to quantify the effect of ethanol on the PM emission formation in the combustion chamber. Thus, in contrast to the common practice of sampling the exhaust gases after they exit from the exhaust pipe, a new sampling system, coupled with a Scanning Mobility Particle Sizer (SMPS) system, has been designed to measure the PM number concentration in the exhaust gases 15 cm away from the engine's exhaust valves. The results and the conclusions are described in Chapter 3.

2.1 Test Matrix

As described in Chapter 1, previous research shows that the majority of PM from DISI engines are emitted during the first minutes of their operation (cold-start-fast-idling period). In this study, in order to measure the effect of ethanol on the PM formation during the combustion process in a DISI engine under cold-start conditions, blends of gasoline and ethanol in different percentages were used as fuels, and the emitted PM was measured for a

range of temperatures from 0°C to 40°C (Table 2.1).

Table 2.1. *Experimental Matrix: how Ethanol content in the fuel and engine's temperature affects the total PN and PN distribution.*

	E0	E2.5	E5	E10	E25	E50	E85
0°C							
7°C							
15°C							
20°C				?			
30°C							
40°C							

Each fuel blend is characterized by the letter E and a number. Thus, E"x" means that x% by volume of the fuel is pure ethanol (CH_3CH_2OH) and (100-x)% by volume of the fuel is gasoline (i.e., E0 is pure gasoline, E5 is 5% vol. ethanol and 95% vol. gasoline, etc.). The gasoline fuel used for the experiments is an EPA Tier II gasoline fuel made by Haltermann: HF0437 (Appendix B). More details about the mixing process are provided later in this chapter. Two heat exchange systems have been used to maintain the temperature of the engine's coolant, fuel and oil at specific values, simulating different cold-start conditions. The temperature range present in the matrix refers to the engine's inlet coolant temperature. During the sampling process, the engine operates under steady state conditions (low load) due to limitations from the instrumentation (SMPS).

Based on the higher oxygenate content of ethanol, the hypothesis to be verified and measured is that, by increasing the ethanol percentage in the fuel, the total emitted PM will decrease for the tested temperature range. When the engine works under lower temperatures it is expected to produce more PM compared to higher temperature operation. The experimental apparatus, described in the following paragraphs tests the above hypothesis.

2.2 Engine Description

The experiments have been conducted on a 2002 production GM Ecotec 2.2 L, a naturally aspirated, DISI, 4-cylinder engine, which has been modified for single cylinder operation (Figure 2.1, Table 2.2).

Figure 2.1. *The DI version of GM Ecotec 2.2L was used in European GM models (Opel Signum, Opel Vectra) in early 2000's.*

Table 2.2. *Engine's Specification*

Displaced volume per cylinder	550 cc
Stroke	94.6 mm
Bore	86 mm
Compression ratio	12:1
Number of Valves	4
Exhaust Valve Open	4.5° BBDC *
Exhaust Valve Close	10.5° ATDC *
Inlet Valve Open	0° ATDC *
Inlet Valve Close	60° ABDC
Injector Center Line	47° from horizontal
Nominal Cone Angle (figure 2.4)	52°

The values that are marked with a * in Table 2.2 have been taken from an internal GM-Opel paper and have not been confirmed for the particular engine. The intake valve closing time has been experimentally verified by measurement of the in-cylinder pressure. The pressure trace shows a small discontinuity when the valve lands on its seat (Figure 2.2).

The engine has four valves, two intake valves and two exhaust valves. The spark plug is centrally mounted and the injector is located on the side of the chamber between the intake valves (Figure 2.3). The engine is a first-generation, air-guided DISI engine, designed for homogeneous operation; hence the piston is flat. Finally, the engine utilizes SIEMENS injectors with a variable operating pressure ranging between 40 and 120 bar. The Injectors' centerline has a 47° angle with the head of the engine, and the fuel spray has a nominal cone angle of 52° (Figure 2.4). Although there is no information from GM-Opel about whether

the injectors are swirl injectors or simply multi-hole, it is known that SMD is less than 16 μm.

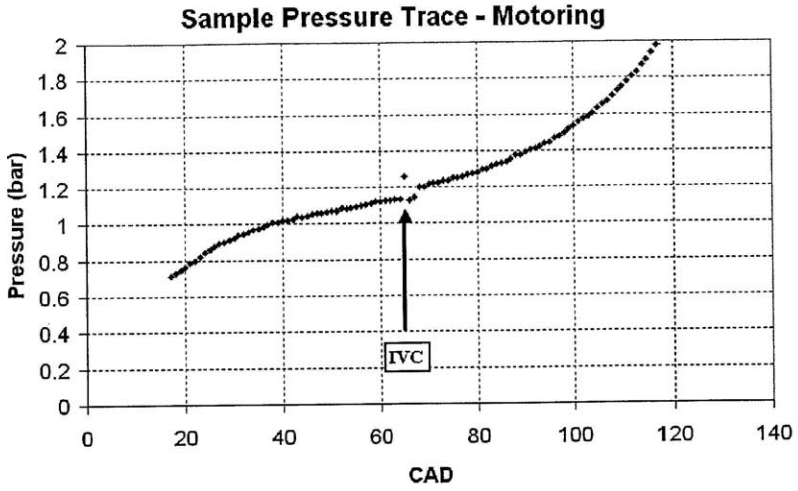

Figure 2.2. *At 65° after Top Dead Center there is a small pressure discontinuity due to the closing of the intake valves.*

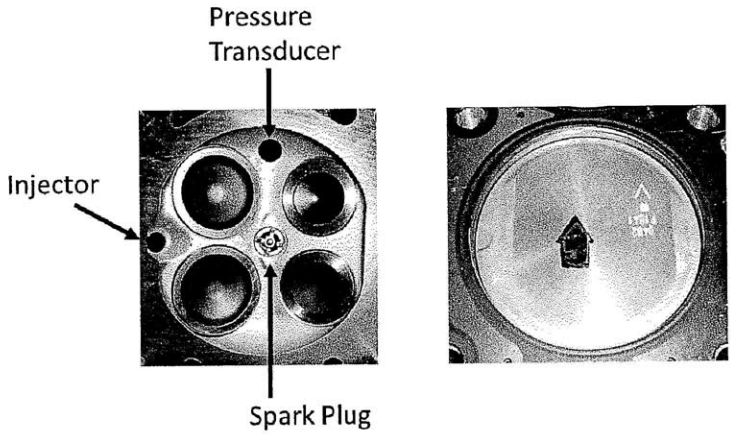

Figure 2.3. *View of the top of the combustion chamber and the top of the piston. The cylinder head is modified in order to accept a pressure transducer that measures in-cylinder pressures during the engine's operation. The piston is flat, designed for homogeneous combustion.*

In order to maximize mixing while allowing for the engine to effectively operate at wide open throttle, the engine employs a charge motion control valve (CMCV). At low speeds the CMCV is closed; thus the air channel, which is parallel to the piston motion, is blocked and the entire charge enters the cylinder through one valve with a swirling motion, producing

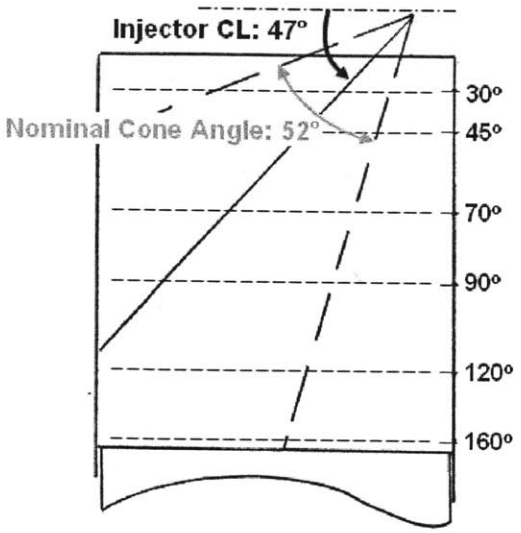

Figure 2.4. *Side view of the cylinder, where the dotted lines indicate the position of the piston for several crank angles.*

better mixing with the fuel (Figure 2.5). For higher speeds, the CMCV is open and the intake air that enters from both intake ports has a tumbling motion, which results in a smaller heat loss. During the experiments, the engine operational condition simulated the cold-start period with low load steady operation; thus the CMCV was kept closed.

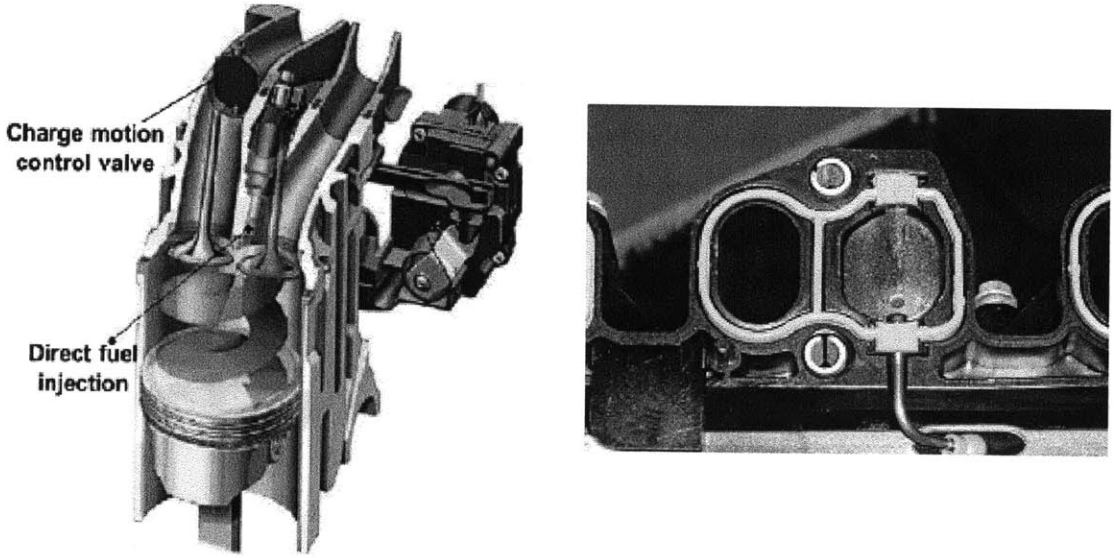

Figure 2.5. *By maintaining the charge motion control valve closed the intake air enters the cylinder with a swirling motion, which results to better mixing with the fuel at low speeds.*

The engine has been modified to run on one cylinder: the cylinder that drives the engine has separate intake and exhaust tubing from the three driven cylinders. The intake air enters the driver cylinder via an air filter. The Manifold Absolute Pressure (MAP) is controlled by two gate valves to inhibit the flow of the intake air: one for large changes and one for fine tuning. A pressure transducer and a thermocouple mounted close to the intake valves indicate the MAP and the air intake temperature for all operational conditions. In order to avoid pulsation from the restricted flow after the two valves, there is a damping tank.

2.2.1 Fuel System

According to the manufacturer, the engine uses a mechanical fuel pump driven by the camshaft to pressurize the fuel prior to injection. However, in order to maintain the chosen injection pressure constant during the experiments, independent of engine speed or other operational parameters, the following set-up has been used: After their preparation, the fuels were stored in hydraulic accumulators. The hydraulic accumulator is a cylinder with an internal piston, capable of sustaining high pressures. At the lower part of the cylinder is the fuel and at the upper part of the cylinder is a gas (in this case the gas used was N_2). The top of the accumulator is connected with a high pressure nitrogen bottle (maximum pressure: 160 [bar]) and a manual pressure regulator (Figure 2.6). The pressure regulator allows nitrogen gas to fill the upper part of the accumulator until the desired pressure is reached, at which point the flow stops. As fuel is injected into the cylinder the fuel level falls and additional nitrogen gas enters the top of the accumulator to maintain the desired pressure. The pressurized fuel from the accumulator enters the fuel rail, via a heat exchanger, and it is injected into the active cylinder through the high pressure injectors. The purpose of the heat exchanger is to maintain the temperature of the fuel close to the temperature of the engine and thus simulate the steady operational condition. The system is limited to an operating pressure of 135 bar (or 2000 psi) by the strength of the stainless steal tubing which was used for the high pressure lines and by the fuel injectors. Since the lines are stainless steal there is little potential for corrosion by the ethanol fuels.

Fuel Preparation Procedure: Each fuel blend was prepared separately. After we measured the volume of the gasoline and of the ethanol, using a graduated cylinder (with accuracy of $\pm 5\%$), the substances were to pour into the fuel tank, where they were mixed (Figure 2.7). The fuel tank is connected to the lower side of the accumulators via a fuel filter and an electric fuel pump. Each accumulator had a valve at the lower side, allowing the user to

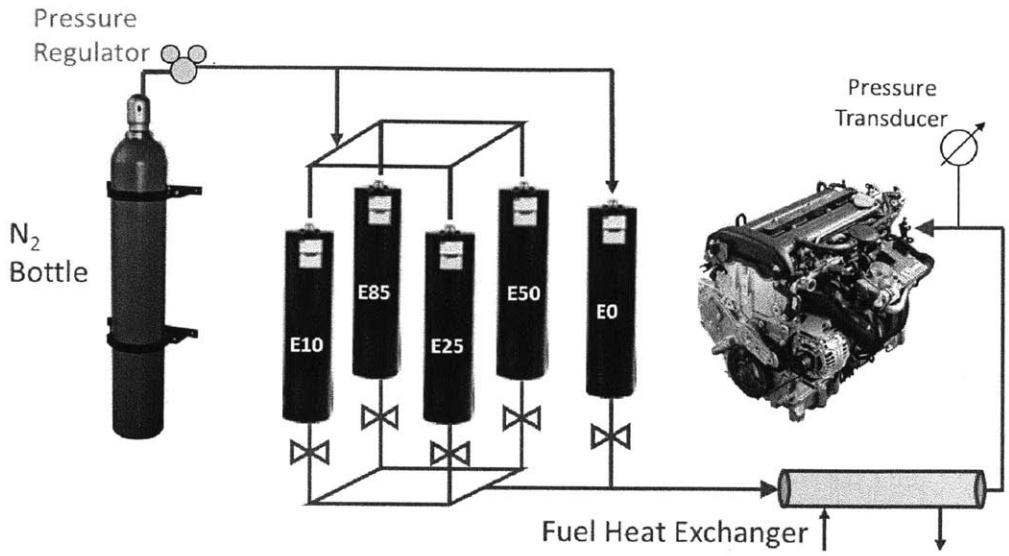

Figure 2.6. *The fuels are stored in hydraulic accumulators. N_2 gas presses the piston of the accumulator with constant pressure independently from the operational condition of the engine. The fuel is maintain close to the temperature of the engine via a heat exchanger using the coolant of the engine.*

choose the one to fill (Figure 2.7 valves 6, 7, 8, 9 and 10). Before starting the fuel pump to fill an accumulator, the tubing system with the nitrogen gas was emptied, to maximize the capacity of the accumulator. As the fuel was pumped into the accumulator, the piston rose with the level of fuel until it reached the upper stops. Before each test with different fuel, the residual fuel and the air from the previous run in the fuel lines needs to be removed. Thus, a N726FTP diaphragm vacuum pump was used to empty the fuel lines and prevent the mixing between the fuels.

Example: If we want to fill the E10 accumulator we should empty the N_2 line and the fuel line and then, before we turn on the fuel pump, we should set the valves of the fuel system, as presented in Table 2.3.

The fuel pressure was not one of the parameters tested during this set of experiments. From previous research on this engine, HC emissions as a function of fuel pressure for UTG91 suggest an optimum fuel pressure (lower HC emissions) around 60 psi (Figure 2.8). That optimum pressure comes from the balance of fuel droplets' size and velocity. Generally, high pressure results in smaller fuel droplets, and thus faster evaporation, but also yields higher velocities, which may cause fuel droplets to hit the wall and thus higher emissions. The

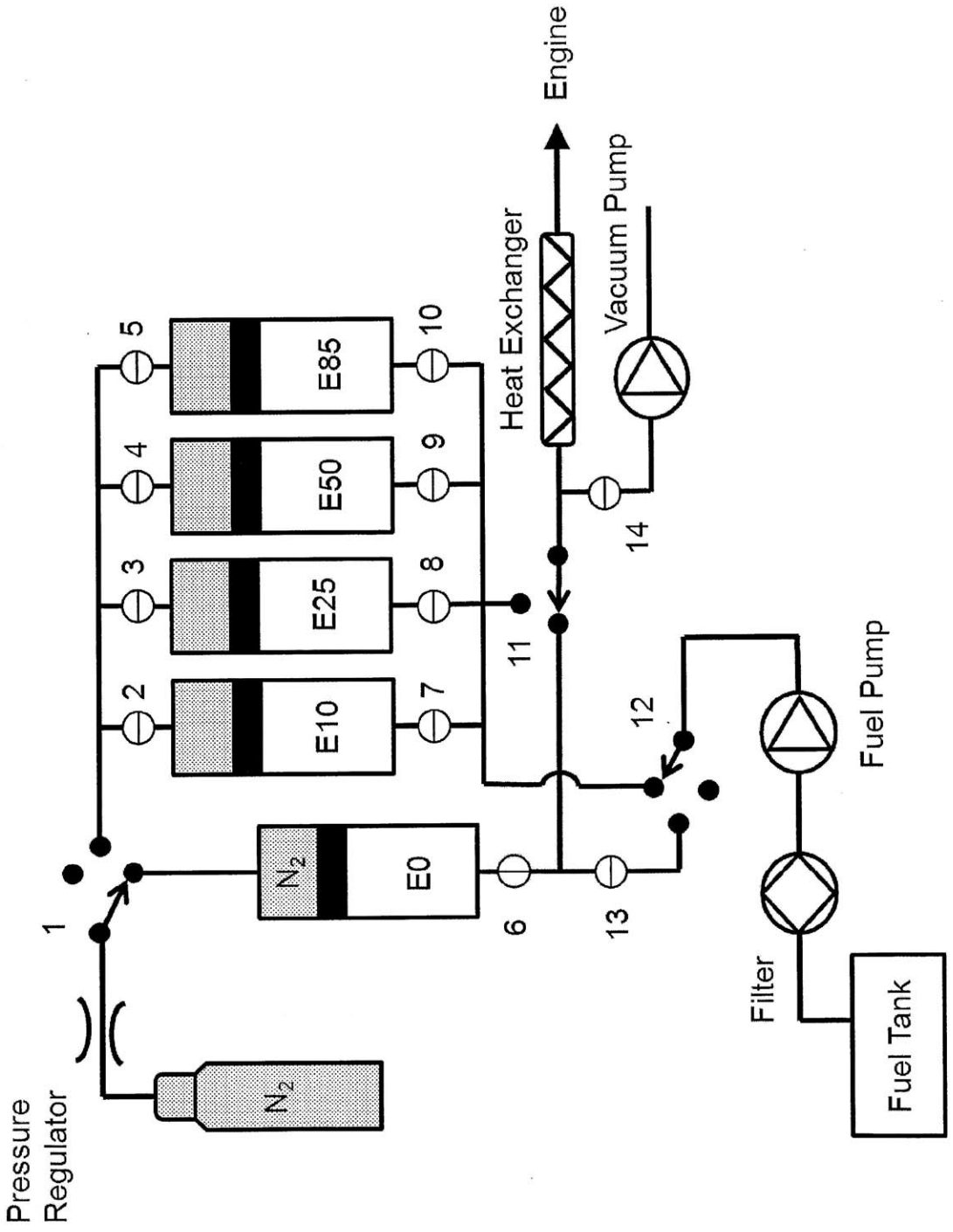

Figure 2.7. *The set up of the fuel system's valves while using E0: The N_2 pressurizes the E0 accumulator and the gasoline is leaded through valve 6, 11 and through the heat exchanger to the fuel rail.*

Table 2.3. *Fuel system's valve set-up to fill the E10 accumulator.*

Valve Number	Valve Position
1	Up
2	Open
3,4,5	Close
7	Open
6,8,9,10	Close
11	Down
12	Up
13,14	Close

opposite effects happen at lower fuel pressures. Hence, the constant fuel pressure chosen for these experiments is 70 bar. The injectors were calibrated as a function of fuel type.

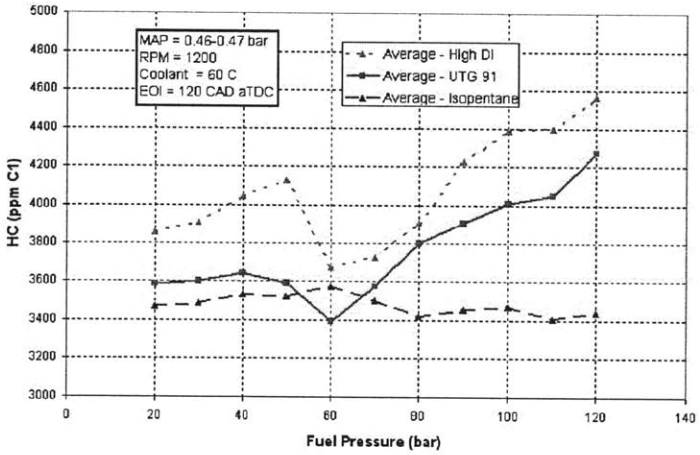

Figure 2.8. *For UTG91 (continuous line), a fuel similar to E0, an optimum fuel pressure appears around 60 psi.*

Another parameter, related to the fuel, that may affect the PM emissions (in both mass and numbers) is the time allowed for mixing between the intake air and the fuel. During these experiments, this time is defined when the user selects the End-of-Injection (EOI) timing at the software used to control the engine. This parameter was not been investigated during this set of experiments; thus the same value for EOI was maintained for all experiments. From previous research, the HC emissions as a function of EOI for three different fuel pressures indicate that for EOI around 110° after Top Dead Center (aTDC) the emissions are minimum for all fuel pressure range (30 - 120 bar). If the injection stops very early, the piston is high, close to the injector, and the higher emissions are due to the impingement of the fuel on the top of the piston (Figure 2.4). For very late EOI timings, the higher emissions are caused

by insufficient mixing of the fuel with the charge. In order to verify that the PM emissions follow the same trend with the HC emissions, the PN distributions for three different EOI (at fuel pressure of 70 bar) were measured (Figure 2.10). For EOI at 110° after TDC, the PM formation is much less than 50° earlier and 50° later. From the data in Figure 2.10 we may conclude that fuel impingement results in an order of magnitude more PM than a bad mixing effect at the specific conditions. During all the experiments the EOI timing was maintained at 120° after TDC.

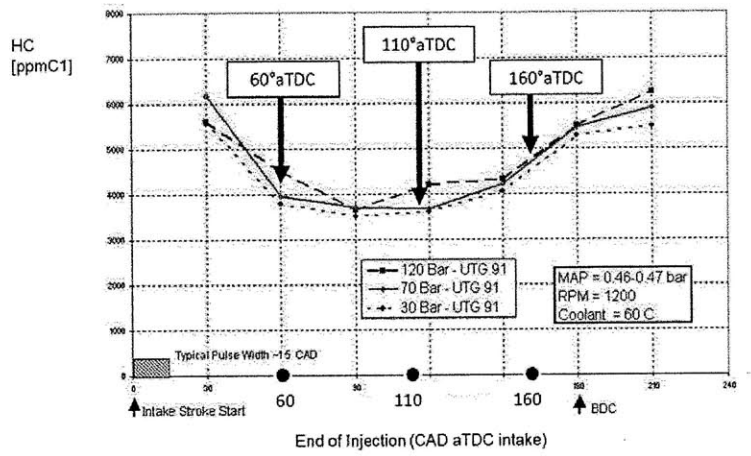

Figure 2.9. *When UTG91, a fuel similar to E0, is injected at 70 bar (continuous line) with EOI timing between 60° and 140° after TDC, the hydrocarbon emissions are minimum.*

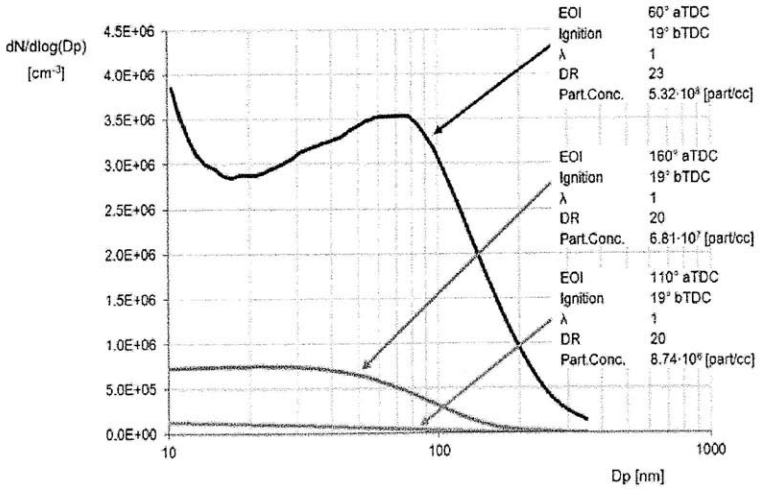

Figure 2.10. *The total PN emitted for EOI timing around 110° after TDC are at least an order of magnitude less than the total PN emitted at 60° and at 160° after TDC.*

2.2.2 Coolant System

A coolant system has been designed to maintain the engine, the fuel, and the oil at constant temperature during the experiments, in order to simulate a variety of cold start temperatures. Two subsystems were used: one for temperatures between -10°C and 25°C (low temperature range) and one for temperatures between 25°C and 90°C (high temperature range). Both subsystems are connected to the engine's coolant system, and to two heat exchangers (one for the fuel and one for the oil), in parallel; therefore only one of them can be used at a time (Figure 2.11).

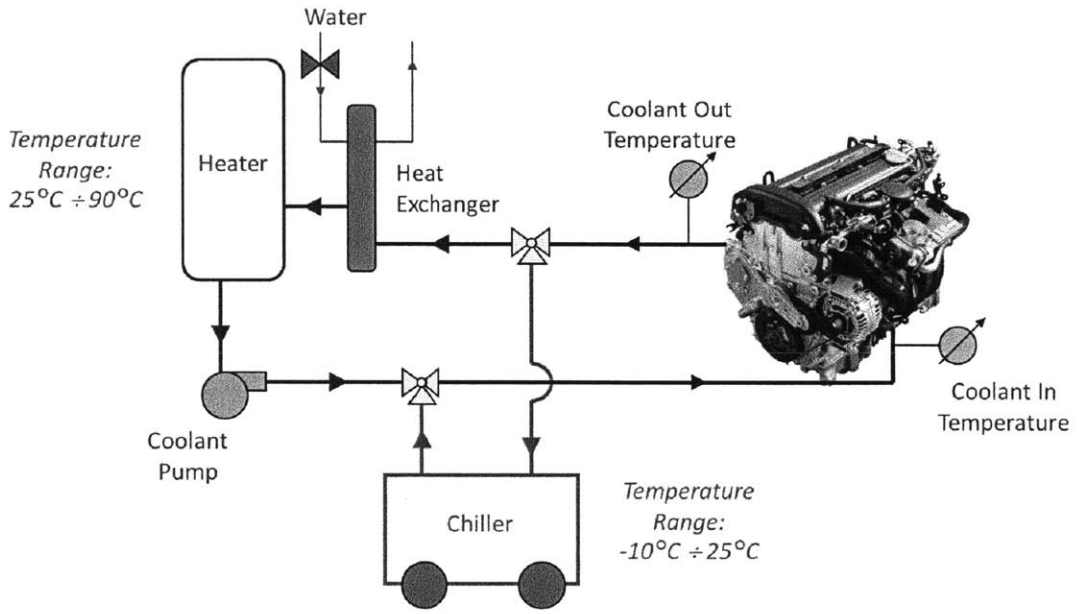

Figure 2.11. *With two subsystems in parallel connection, we could vary the temperature of the engine from -15° C up to 90° C.*

The high temperature range has been achieved with the use of a 10 KW electric heater. The electric heater provides a relatively quick ramp-up of the coolant temperature when activated. The subsystem was coupled with a line from the city's water supply and a solenoid valve in order to maintain the desired temperature constant: when the engine was operated at high temperatures, two set-points were used to bracket the desired temperature. If the coolant temperature was less than the first set-point, the electric heater would be activated to increase the coolant temperature. If the coolant temperature exceeded the second set-point, the solenoid would close and allow city water to flow into the heat exchanger where it would serve to reduce the temperature of the coolant.

For the low temperature range a chiller, was used. The engine's coolant fluid exchanges heat with Freon-13 in the chiller and it is pumped back to the coolant system via an electric pump. The chiller has a temperature closed loop control system, allowing the user to accurately set and control the desired temperature.

2.3 Main Instrumentation and Data Acquisition System

A series of instruments and measuring devices have been used in order to run and monitor the experiments. Most of them are commonly used in the industry and in labs (such as OMEGA K-type thermocouples, pressure transducers, flow meters, etc) and there will not be analyzed in this section, with the exception of two sensors: the in-cylinder pressure transducer and the lambda meter). The last part of this section presents the data acquisition system used to control and monitor the engine's operation.

In-cylinder pressure transducer

A Kistler 6125A piezoelectric pressure transducer was used to measure the cylinder pressure (Figure 2.12. This particular sensor has fast response and is broadly used by the industry and academics for this type of application. In order to measure cylinder pressure, the sensor had to be mounted inside the engine head. It was very important that this complex machining be done precisely. The machined section had to reach a precise depth in order to minimize the separation between the tip of the sensor and the combustion chamber to ensure a fast and accurate response. At the same time it was critical that the contour of the combustion chamber and its structural integrity not be compromised or else the potential existed for a catastrophic mechanical failure which would not only damage the engine but also pose a risk to anyone near the engine. It was also important to properly isolate the pressure transducer from coolant and oil galleries. Due to the complexity and tight tolerances of this machining, it was performed by GM at their facilities.

The pressure sensor is a relative measurement device to determine the pressure in the cylinder, the output of the sensor at a given time must be pegged to a known value. This is done through the use of a secondary pressure sensor located in the intake manifold which records the manifold pressure (MAP). The output of the pressure transducer at BDC of the intake

stroke is "pegged" at the pressure determined by the pressure sensor in the manifold. The linear relationship between pressure and the output of the pressure transducer allows the change in pressure to be found, which is then added to the MAP to determine the cylinder pressure.

Figure 2.12. *The pressure transducer used to measure the in-cylinder pressure is the Kistler 615C model. It has a sensitivity of 13.7 pC/bar with a linearity of ±0.5% of the full scale.*

Lambda Meter

To acquire air/fuel ratio information, an Etas LA4 Lambda meter was located 17 cm from the exhaust port. The meter utilizes a Nernst concentration cell and an oxygen ion pump cell. The meter is has a planar two cell design with one layer composed of a solid body multilayered ceramic electrolyte which separates a reference gas and the exhaust. The difference in oxygen concentration between the reference gas and the exhaust is a function of the air/fuel ratio of the combustive mixture in the cylinder. A voltage is induced across the electrolyte which is very sensitive to the difference in oxygen concentration. The precise measuring of this voltage allows the lambda sensor to determine the lambda value in the cylinder.

Engine Control System

The engine control system consists of a master and slave computer. The master computer accepts the user inputs of engine speed (RPM), target lambda value, end of injection (EOI, in CAD aBDC compression), and spark timing (CAD aBDC compression). A program, written in C, calculates the start of injection (SOI) and the dwell in crank angle degrees. The dwell is the amount of time that the spark plug needs to be charged before it emits its spark. The master program places this information into an array which is sent to the slave computer.

The slave computer must run its C program in DOS since the computations for small actions, like moving the mouse, have the potential to cause the outputs enough delay that the engine could misfire for a cycle. The slave program accepts the inputs of feedback gain (typically

10) and injection duration (μsec). Then it provides the digital signal for the operation of the injector and the spark plug. A hardware switch is used to interrupt the engine"s operation and ensure that the sequence of injecting and firing is stopped with the injector in the closed position.

Data Acquisition System

The data acquisition system is modeled on a National Instruments platform. The schematic of the hardware is shown in Figure 2.13. A list of the components and their function is provided in Table 2.4 [21]. Several thermocouples have been integrated into the engine to measure properties such as intake and exhaust temperature, coolant temperature and fuel temperature. However, the time response of the thermocouple hardware is not sufficient to allow the data to be logged at the speed at which the engine is running. Thus, the thermocouples were connected to an Omega thermocouple reader separate from the rest of the data.

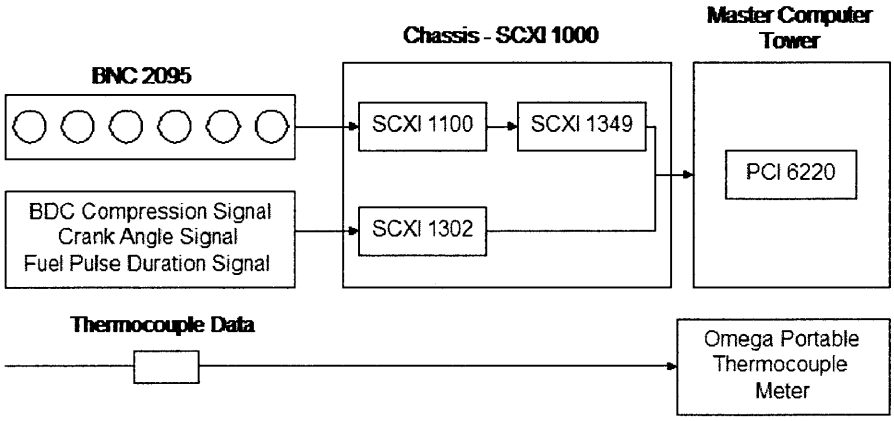

Figure 2.13. *The Data Acquisition System.*

Table 2.4. *The components of the data acquisition system*

Item	Function
BNC 2095	Records up to 16 different analog BNC signals
SCX 1100	Multiplexes the signal into a single program to gain instrumentation amplifier (PGIA)
SCX 1302	Allows digital signals to be feeded to the master computer
SCX 1349	Necessary adaptor to include feed through signals
PCI 6220	Data acquisition card

2.4 PN Measurement Approach

In order to measure the effect of ethanol content in the fuel on PM formation in the combustion chamber, a sampling system has been designed to sample raw exhaust gases only 15 cm after the exhaust valves of the working cylinder, and to minimize particle losses during sampling procedure (Figure 2.14). The sampling system is comprised of a mini-dilution tunnel, using N_2 as dilution gas, coupled with a Scanning Mobility Particle Sizer (SMPS), an instrument that produces the number distribution of the particulate matter in the exhaust gases versus their electrical equivalent diameter (PN distribution). The following paragraphs describe this measuring system and the methodology followed during the experiments.

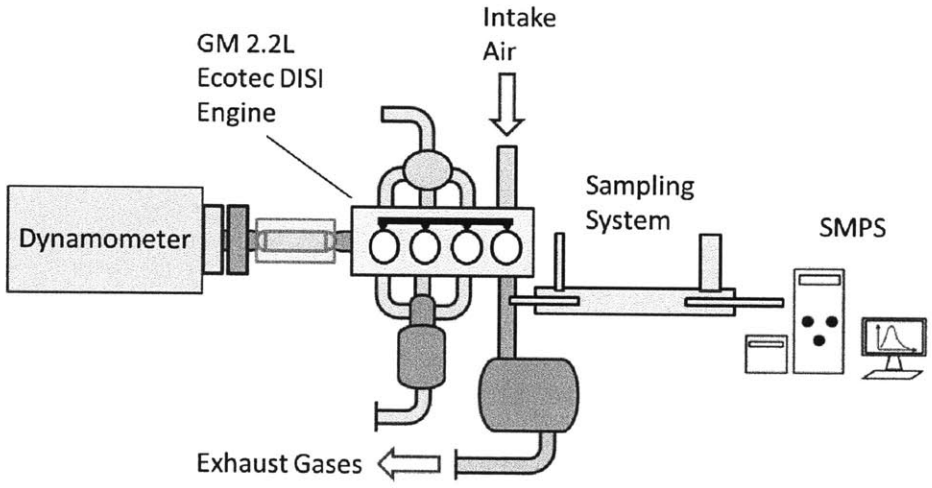

Figure 2.14. *The engine has been modified for one cylinder operation. The exhaust gases, that have been sampled a few centimeters after the working cylinder's exhaust valves, are collected and analyzed by an SMPS system.*

2.4.1 The sampling system

A strategy for measuring PM emissions, commonly used in diesel engines, is to sample the exhaust gases exiting the tailpipe of the vehicle, then dilute them with air in a full dilution tunnel, and finally feed a portion of the diluted exhaust gases into a SMPS to produce their PN distribution as a function of their electrical equivalent diameter. This research focuses on the effect of ethanol on PM formation *in the combustion chamber*, thus a different

approach has followed. The exhaust gases have been sampled only 15 cm downstream from the exhaust valves of the working cylinder. At this point the temperature of the exhaust gas for the cold-start conditions is around 420°C. The PN in the raw exhaust gases exceeds the maximum range of the SMPS, thus the exhaust gas sample needs to be diluted with a particle-free gas. The challenge in the design of a dilution system is to minimize particle losses and the particle size changes during the sampling process.

As mentioned in Chapter 1, there are seven particle losses mechanisms, that we identified and we minimized during our experiements:

a. **Diffusion.** Diffusion losses are easy to predict by calculating the penetration of particle sizes between 10 and 550 nm, using the following formula:

$$P = \frac{n_{out}}{n_{in}} = 1 - 2.56 \cdot \Pi^{2/3} + 1.2 \cdot \Pi + 0.1767 \cdot \Pi^{4/3}, \tag{2.1}$$

for $\Pi = \frac{\pi \cdot D \cdot L}{Q} = \pi \cdot \varepsilon < 0.02$,
where,
P is the penetration (fraction of entering particles that exit the tube),
ε is a dimensionless deposition parameter,
D is the diffusion coefficient ($D = \frac{k \cdot T}{frictioncoefficient}$),
L is the length of the tube,
Q is the volumetric flow rate of the gas [9],[11].

In both tubes, penetration was above 98%, which means that there are practically no particles losses due to diffusion.

b. **Thermophoresis.** In contrast with the diffusion, where there is a direct formula to calculate particles' penetration, in the case of thermophoresis there are theoretical formulas only for calculating the thermophoretic velocity of the particles (a velocity with direction towards the colder surfaces, i.e. the walls), which is difficult to translate to actual particle losses. In our system thermophoresis is significant in the sampling tube, before the dilution stage (a tube 7 in long, with outer diameter of 0.25 in and inner diameter of 0.18 in), due to the high temperature of the exhaust gases flow in a small tube, where the surface area is large relative to the flow area. To keep thermophoretic deposition to a minimum, the sampling tube was maintained as short as possible and the part of the tube that has been exposed to the atmosphere was insulated. However, almost half of the tube was still exposed to the cold dilution gas (N_2). In order to overcome this problem, this part of the sampling tube

has been insulated as well, using a ceramic tube. The ceramic tube was sealed at both ends and the trapped air between the sampling and the ceramic tube provides thermal insulation (Figures 2.15, 2.16).

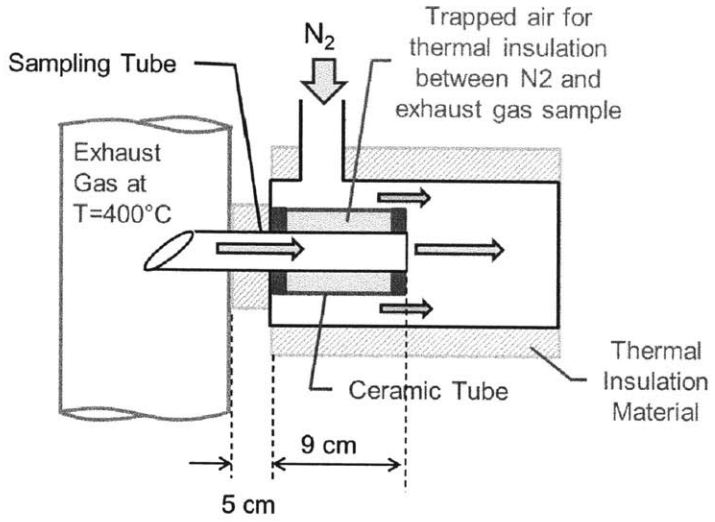

Figure 2.15. *Detail of sampling system: the sampling tube. A ceramic tube has been used to insulate the hot flow of the sampling gas from the cold dilution gas, before the mixing.*

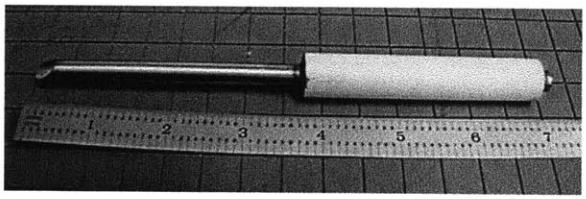

Figure 2.16. *Detail of sampling system: the sampling tube. A ceramic tube has been used to insulate the hot flow of the sampling gas from the cold dilution gas, before the mixing.*

c. **Absorption, Condensation and Coagulation**. In order to minimize these effects we shorten the length of the sampling tube to dilute the raw exhaust gases fast and we introduce a high enough dilution ratio in the mini-dilution tunnel. After the dilution, there are two main effects: a) the distances between the particles will increase, thus the probability for coagulation and absorption is significantly decrease and b) the partial vapor of the gas will increase to avoid any condensation.

d. **Gravitational Deposition**. Gravitational deposition depends on the time the particles spend in any part of a sampling system. This is a very small effect for particles during the

sampling process, because of their very small in size and in mass.

e. **Electrostatic Deposition**. Generally, particles have a natural residual charge from the combustion process. To prevent electrostatic deposition all sampling lines had a common ground with the engine.

For the dilution process a mini-dilution tunnel has been designed, using N_2 as diluter gas (Figure 2.17). A N_2 bottle under pressure provides the dilution gas, which flow is constantly controlled via an OMEGA mass controller, with a variation less than 5% from the desired value. Also, the temperature of the N_2 is controlled using an electrical heating wire and a close control loop with accuracy of less than 1°C (temperature range: 25°C up to 300°C).

The sample of the hot exhaust gases and the N_2 mix in co-axial flow in the beginning of the dilution tunnel, with the N_2 on the perimeter and the raw exhaust in the center of the flow. The dilution tunnel is a insulated tube of 0.75 in OD and 0.62 in ID. After 85 cm of mixing length, only a small part of the diluted exhaust gases is guided to the SMPS. The rest is going out to the exhaust trench via an electric pump. Both the mass flow rates of the diluted exhaust gases going to SMPS and to the exhaust trench are constantly measured and they have been kept constant during the PN distribution curves generation. Finally, in order to accurately measured the dilution ratio during the sampling process, a HORIBA MEXA-324J/554J portable emission analyzer measured the percentage of CO_2 in the exhaust and in the sample just before entering the SMPS system. The dilution ratio is calculated as $DR = \frac{\%\ of\ CO_2\ in\ the\ raw\ exhaust\ gases}{\%\ of\ CO_2\ in\ diluted\ sample\ going\ in\ the\ SMPS}$. The flow rate of the exhaust gases before the dilution has not been measured. Since all the other flow rates had been measured, the flow rate of the exhaust gases before the dilution has been calculated as $Flow_{exhaustgas} = Flow_{totalout} + Flow_{SMPS} + Flow_{HORIBA} - Flow_{N_2}$. The flow rates of the SMPS and the HORIBA gas analyzer are constant.

In order to choose the sampling conditions, a series of tests have been conducted and a experimental protocol was established to validate the SMPS and the mini-dilution tunnel performance. During this set of experiments the engine was running under the operational conditions described in Table 2.5. These conditions have been chosen to ensure a stable engine operation (COV$\leq$2%) and lower PN than those of the actual tests, which are conducted at lower engine coolant temperature. Successful measurement at the lower PN values would guarantee sufficient instrumental sensitivity.

First, for three different days, we measured the PN concentrations under the same engine

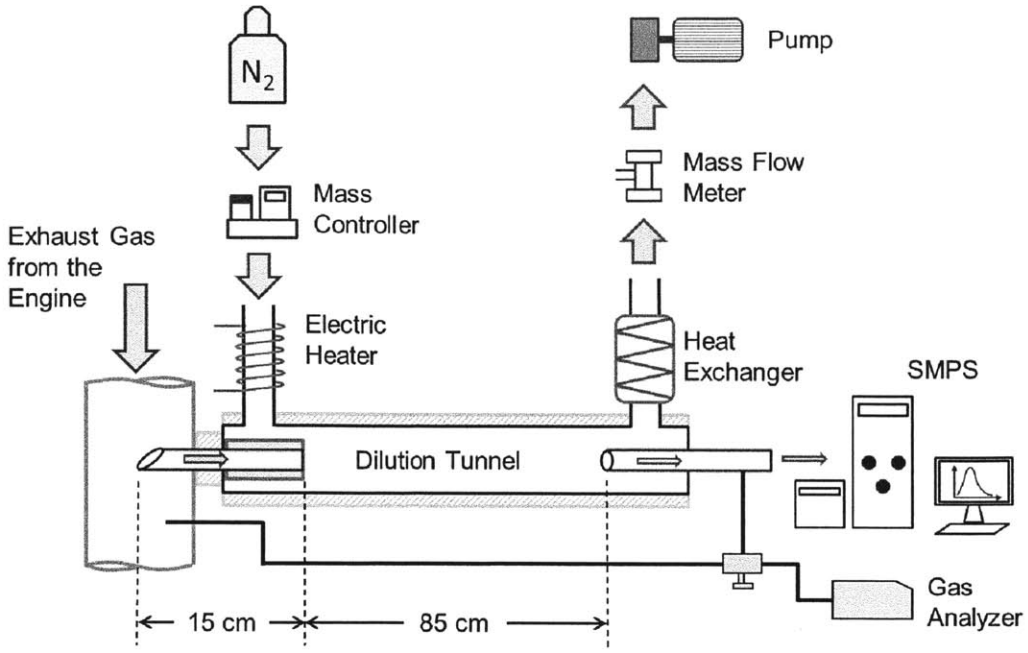

Figure 2.17. *In order to reach the SMPS's measuring range the sample of the exhaust gases has been diluted with nitrogen using a mini-dilution tunnel.*

operational conditions, in order to test the repeatability of the apparatus. From the results in Figure 2.18, we can conclude that our sampling system is repeatable and robust. Each curve is the average from 10 PN distributions and the bars indicate the 90% confidence interval for each case.

Due to the short length of the sampling tube (Figure 2.17), the most significant parameters affecting the PM losses in our process is the dilution ratio and the temperature of the N_2. By varying the temperature of the N_2 from 20°C up to 300°C, while keeping constant all flow rates and constant dilution ratio (DR=40), we can measure any possible losses due to the mixing of the hot exhaust gases with the diluter. From the curves in Figure 2.19 we can conclude that the temperature of N_2 has no effect on the PN distribution. Other studies that sampled from the exhaust tailpipe of the car in order to investigate PN distribution (with exhaust gas temperatures are in the order of 150-200°C), suggest that the chosen temperature of the diluted gas plays an important role for an accurate measurement. In this case, during the dilution process the temperature of the sample exhaust gas is in order of 400°C and is reduced to 40°C fast enough so that the gas does not cross the dew curve and does not suffer from condensation effects that could change the PN distribution.

Table 2.5. *Engine operational conditions during the sampling system validation process*

Fuel	E0 (Gasoline)
Speed	1500 rpm
NIMEP	3.8 bar
Coolant Temperature	80°C
End of Fuel Injection	120° aTDC-intake
Spark Ignition	19° bTDC
Fuel Pressure	70 bar
λ	1 (stoichiometric combustion)

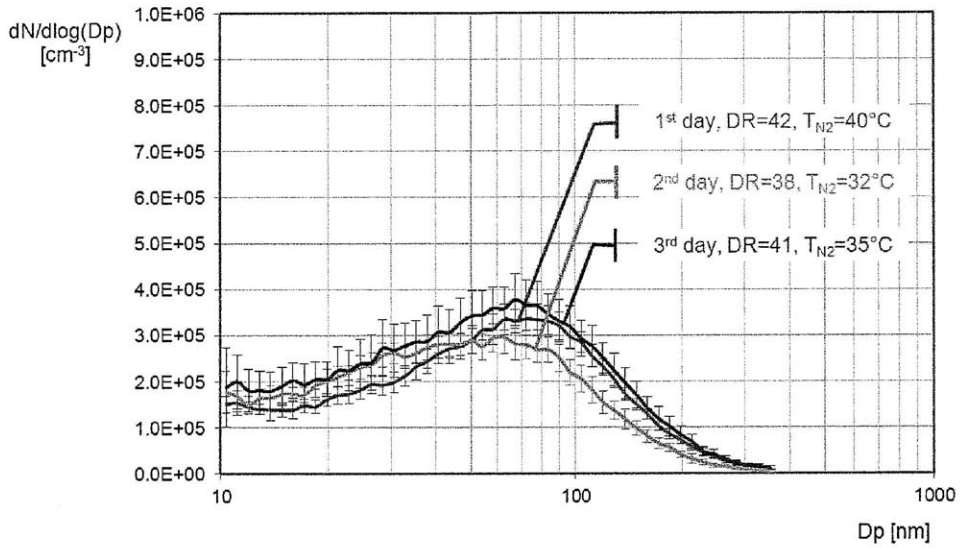

Figure 2.18. *To check the repeatability of the sampling system, the PN distribution for three different days under the same sampling conditions has been plotted. Each line is the average of 10 curves. The error bars represent the 90% confidence interval.*

The second important parameter is the dilution ratio (DR). The DR changes if the flow rate of the diluter (N_2) or the flow rate of the diluted exhaust gases going to to trench changes. From Figure 2.20 we can conclude that for DR$\geq$15, we avoid losses due to coagulation and due to diffusion. That is also a reason for the use of a dilution tunnel: the diluter keeps the particles away from each other, and by increasing their distances we minimize the probability of collision, thus the increase of their size compare to the sampling point (coagulation). Also, by decreasing the relative pressure of the sampling gas, we also decrease the probability for condensation. For DR less than 10 we notice significant decrease of the PN due to these mechanisms.

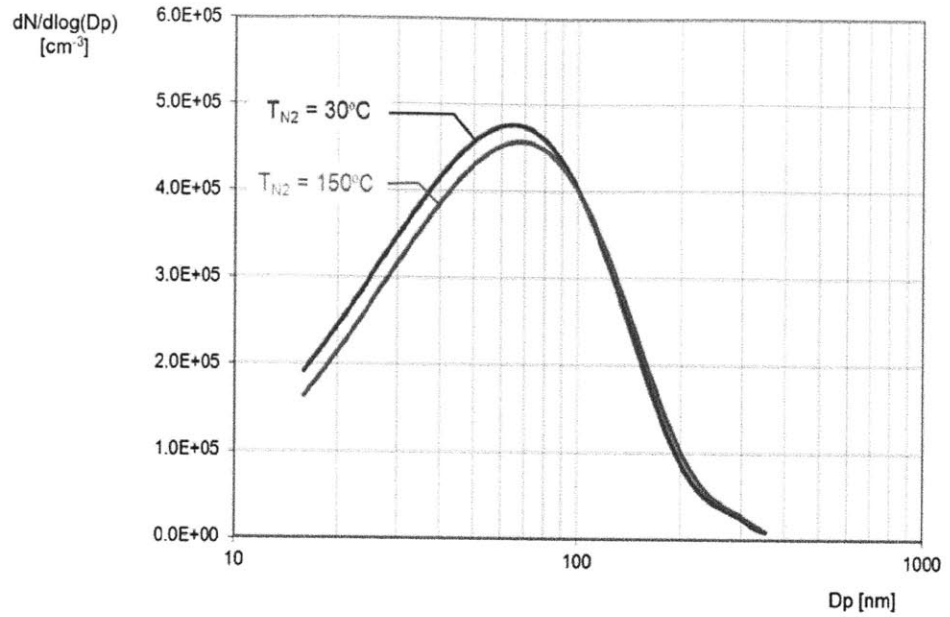

Figure 2.19. *The PN distribution did not changed for the a range of the diluter between 20°C and 300°C (DR=58).*

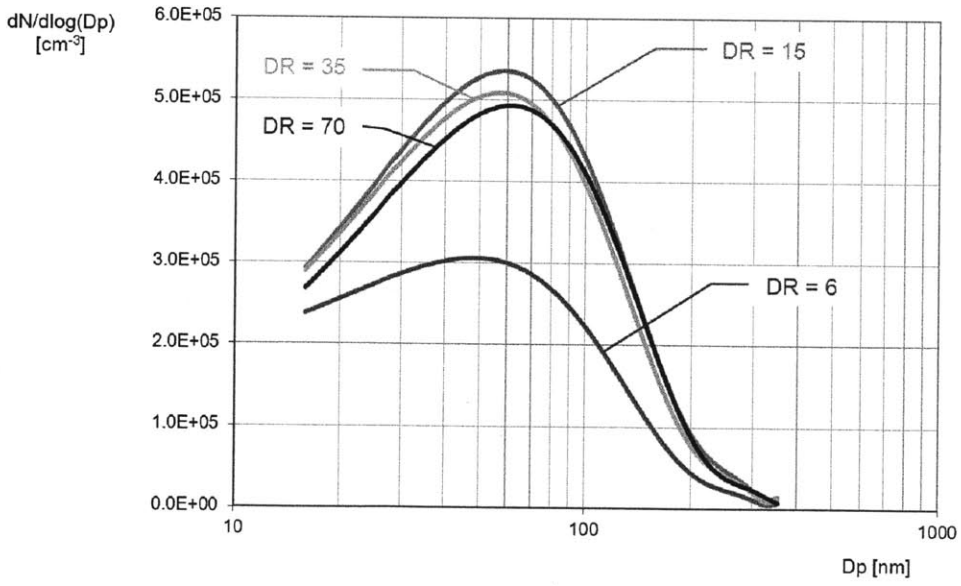

Figure 2.20. *In order to avoid particle losses or change in the PN distribution due to coagulation and condensation, a dilution ratio higher than 20 was maintained during the sampling process.*

The sampling conditions used during our experiments are summarized in the Table 3.1.

Table 2.6. *Sampling system operational conditions*

N_2 flow rate	30 SLPM (±0.3 SLPM)
N_2 temperature	30°C (±2°C)
SMPS sample flow rate	0.7 LPM (±0.1 LPM)
Pump flow rate	23.5 SLPM (±0.1 LPM)
dilution ratio	30:1

2.4.2 The SMPS system

For measuring the size of particles smaller than 1 micron, one of the techniques is based on the different electrical mobilities of different particles' sizes, when they are charged. Systems of this type have existed since the 1960's with the most widely used current instrument being the Scanning Mobility Particle Sizer (SMPS) system, manufactured by Trust, Science, Innovation Incorporated (TSI) (Figure 2.21). The SMPS system gives high size resolution but requires a stable aerosol flow for a minimum of 30 seconds (with longer test times being more common), in order to plot each size distribution measurement. That is the main reason for the steady-state approach to simulate the transient period of cold-start operation of the engine.

Figure 2.21. *During the experiments the SMPS 3934 system has been used to produce the Particulate Number concentration distribution. This system has two main subsystems: the 3071A Electrical classifier that charges the particles and allows only a specific size range of them to enter to the 3010 CPC unit, where there are counted based on their size.*

The SMPS system we used for our experiments is the TSI 3934 model, which consists of two main components: the electrical classifier, model 3071A, and the condensation particle sizer unit, model 3010.

How the SMPS works

The sample of the exhaust gas (or in general the polydisperse aerosol) enters the electrical classifier after it passes the first classifier, an impactor. Depending on the size of the impactor, only aerosol particles below a known size (cut-point aerodynamic diameter) are allowed to pass. The rest are removed by inertial impaction: a nozzle accelerates the polydisperse aerosol in the impactor, which is then forced to turn 90°. The larger particles hit the impactor plate and stay there, in contrast with the smaller ones, which follow the streamlines of the flow and enter the electrical classifier (Figure 2.22).

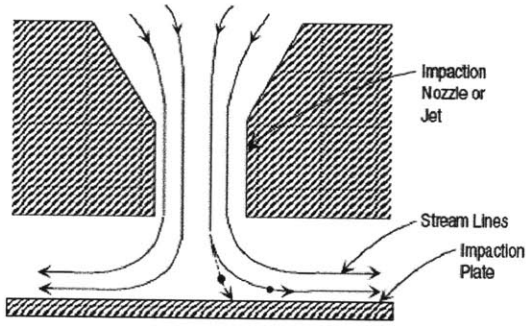

Figure 2.22. *The impactor used in the SMPS system is to remove particles larger than a known aerodynamic size.The rest are entering into the electrical classifier.*

The aerosol that enters the electrical classifier is exposed to high concentration biopolar ions from a Kr-85 bipolar charger. After the charger, the particles attain a bipolar charge distribution, based on their size. The charged particles enter the differential mobility analyzer (DMA) together with filtered air (sheath air). As they enter, the electrical field between a collective rod in the middle and the outer cylinder (housing) of the DMA attract the particles towards the collective rod. The larger particles have higher electrical mobility and they are collected on the surface of the rod. Particles with low electrical mobility leave the DMA (excess air). Particles within an intermediate range of electrical mobilities exit with the monodisperse flow through a small slit at the bottom of the collector rod and they go to the condensation particle counter (CPC).

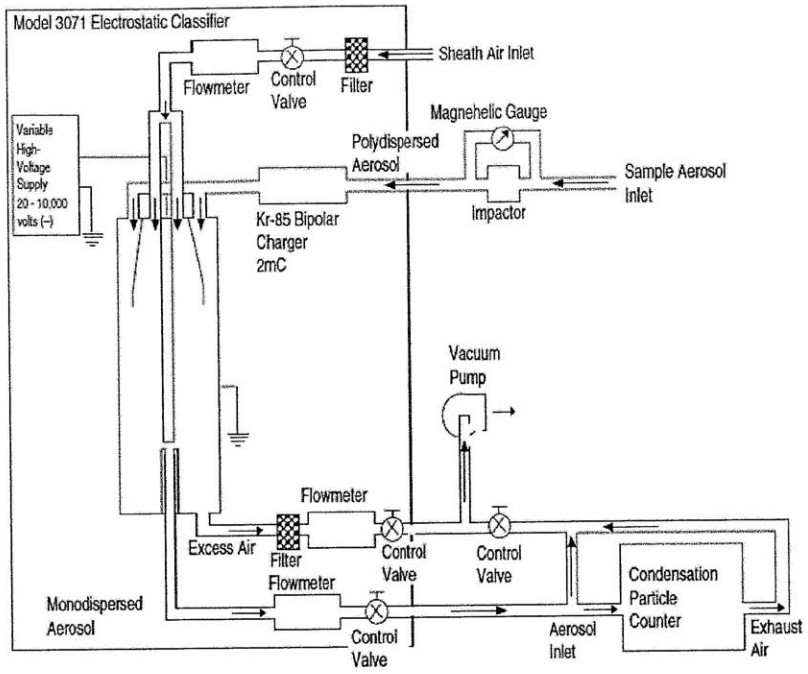

Figure 2.23. *The main components of the SMPS system: Impactor, electrical classifier and CPC unit.*

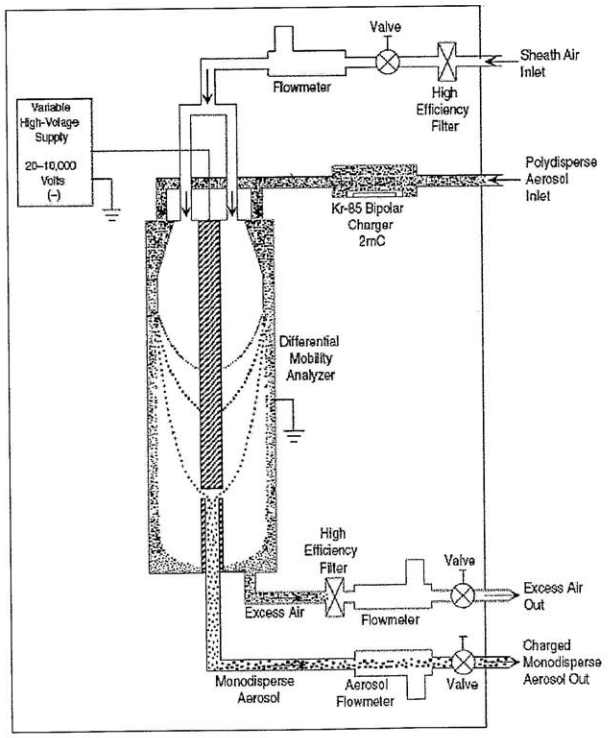

Figure 2.24

The charged particles leaving from the Bipolar charger are mixing with the sheath air into the Differential Mobility Analyzer (DMA). The particles with sizes within the preadjusted range (monodisperse aerosol) leaving the Electrostaic Classifier to enter the CPC unit. The particles that have not trapped in the DMA are leaving the apparatus (excess air).

The monodisperse aerosol from the classifier enters the CPC, where it is saturated with alcohol as it is passed over a heated pool of alcohol. The vapor-saturated alcohol aerosol then flows through the cold condenser, in which it is cooled by thermal diffusion. The alcohol condenses onto the aerosol particles and particles grow up into droplets large enough to be optically counted (laser beams). The CPC unit is connected to a computer, where the PN distribution of the monodisperse aerosol is produced and displayed.

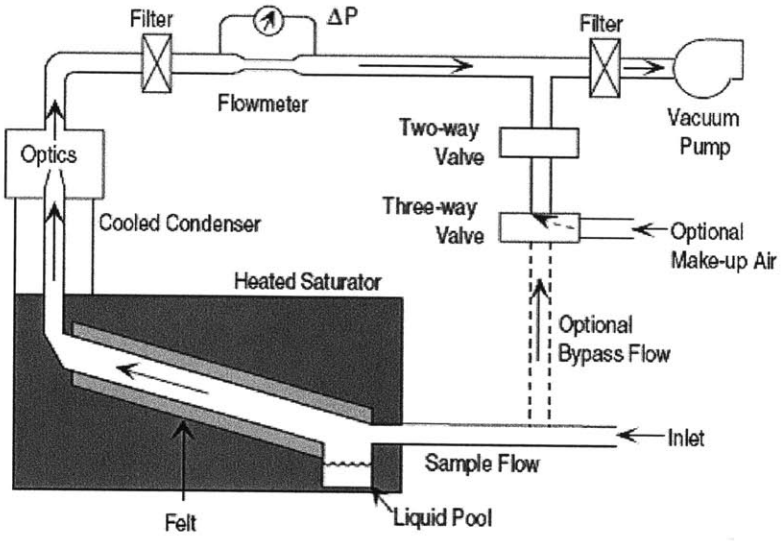

Figure 2.25. *The monodisperse aerosol that enters the CPC unit pass through ethanol vapor and they grow in size. Then the particles are counted as they pass through a set of laser beams.*

Chapter 3

Experimental Results and Conclusions

Using the experimental apparatus and the methodology described in Chapter 2, we tested seven different blends of ethanol-gasoline as a PM reduction strategy for DISI engines during cold-start operating condition (Table 3.1). In this chapter we present and analyze the effect of engine temperature, as well as the effect of ethanol content in the fuel on PM formation in the combustion chamber. The focus of this work is the emitted particles number concentrations. The chapter ends with the conclusions from this research and with suggestions for future work.

Table 3.1. *Engine operational conditions for tested engine temperatures and gasohol blends.*

Speed	1200 rpm
NIMEP	1.5 bar
End of Fuel Injection	120° aTDC-intake
Spark Ignition	15° bTDC
Fuel Pressure	70 bar
λ	1 (stoichiometric combustion)

3.1 The effect of engine temperature on PM formation

The temperature range for which we tested the fuels is between 0 and 40°C. Data presented in this section is the PM size distributions measured with SMPS for the following fuels:

E0 (gasoline), E10, E25, E50 and E85. PM size is based on particles' electrical mobility equivalent diameter (D_p), which ranges from 15 up to 350 nm. The y-axis is the PM number concentration, normalized with the differential interval of the logarithm of particle size ($dN/dlogD_p$). A logarithmic scale is used on both axes because the data spans several orders of magnitude. The distributions shown are time-averaged during 15 mins of steady-state engine operating conditions.

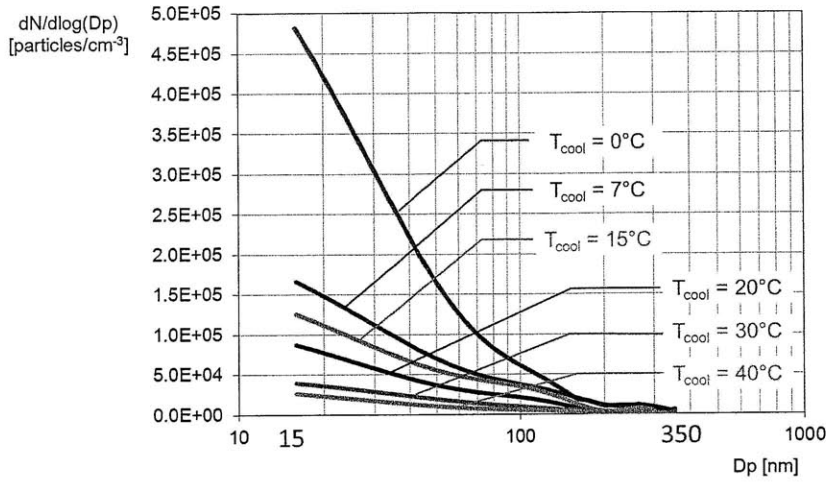

Figure 3.1. *Even though temperatures vary, the shape of the PN distribution remains the same. As temperatures decrease, the emitted PN increases.*

Before we present PN distributions for ethanol blends we can draw the following conclusions related to the gasoline (E0) case:

1. The shape of the PN distribution for E0 is the same for all temperatures and for the operating conditions described in Table 3.1. However, by comparison with the PN distributions presented in Figures 2.18, 2.19 and 2.20, which present the PN for gasoline as well, we observe a different shape. The difference between the two cases is the engine operating conditions (Table 2.5 vs. Table 3.1). Thus, the shape of the distribution is related more to engine operating conditions (ignition and injection timing, load, speed) than engine temperature.

2. The differences in PN are observed for $D_p < 150$ nm (ultrafine- and nano-particles). In general, we found that at the chosen sampling point, the numbers of smaller particles influence the distribution more than the bigger ones.

3. The general trend is that as engine temperatures decrease, the emitted PM increases. For engine temperatures higher than 20°C, PN distributions do not change significantly.

However, for temperatures from 20°C down to 7°C, we observe a distinct increase in PM emissions. Finally, at 0°C, we observe a 3-times higher PM emission compared to 7°C. A possible explanation for this is that, at higher temperatures, the fuel evaporates faster, and thus mechanisms for PM formation, such as fuel impingement, are suppressed.

The following figures are the PN distributions for the tested gasohol blends:

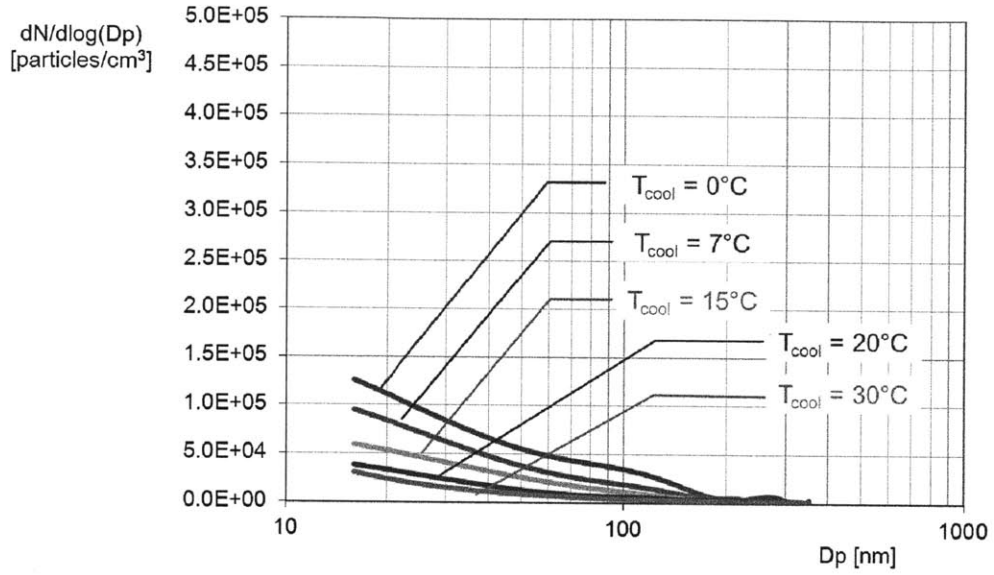

Figure 3.2. *The PN distribution under cold-start conditions for* ***E10*** *(10% by vol. ethanol. and 90% by vol. gasoline).*

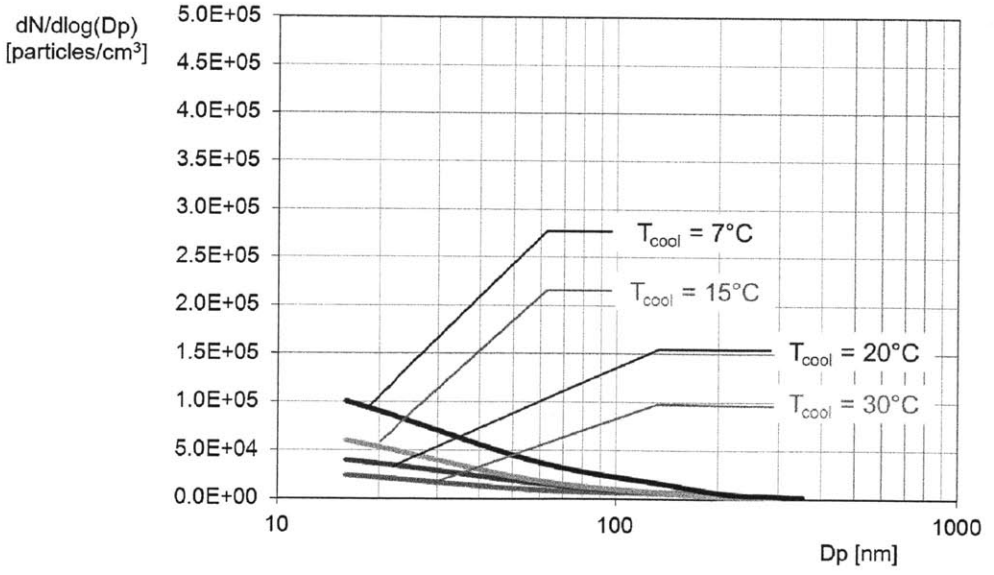

Figure 3.3. *The PN distribution under cold-start conditions for* ***E25*** *(25% by vol. ethanol. and 75% by vol. gasoline).*

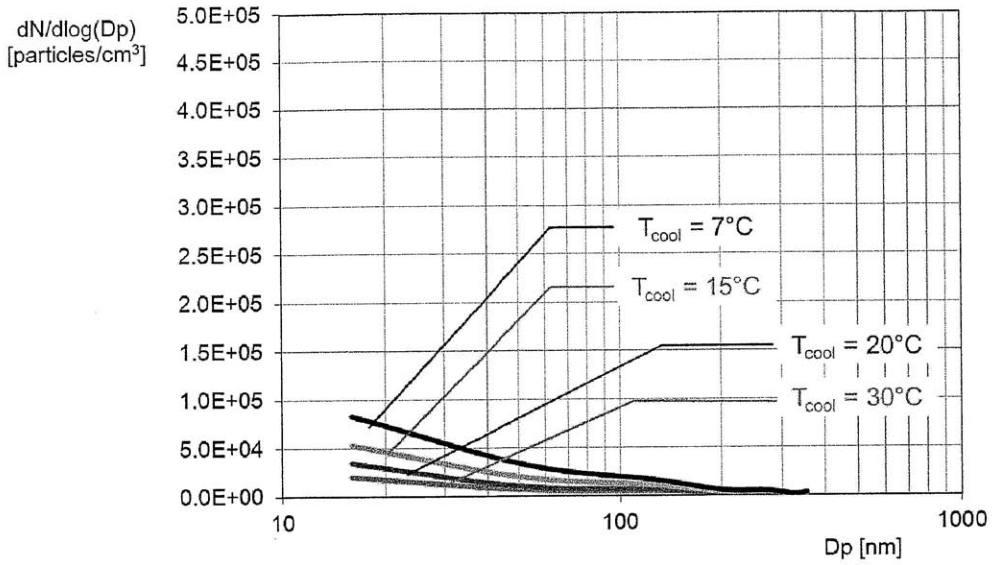

Figure 3.4. *The PN distribution under cold-start conditions for* ***E50*** *(50% by vol. ethanol. and 50% by vol. gasoline).*

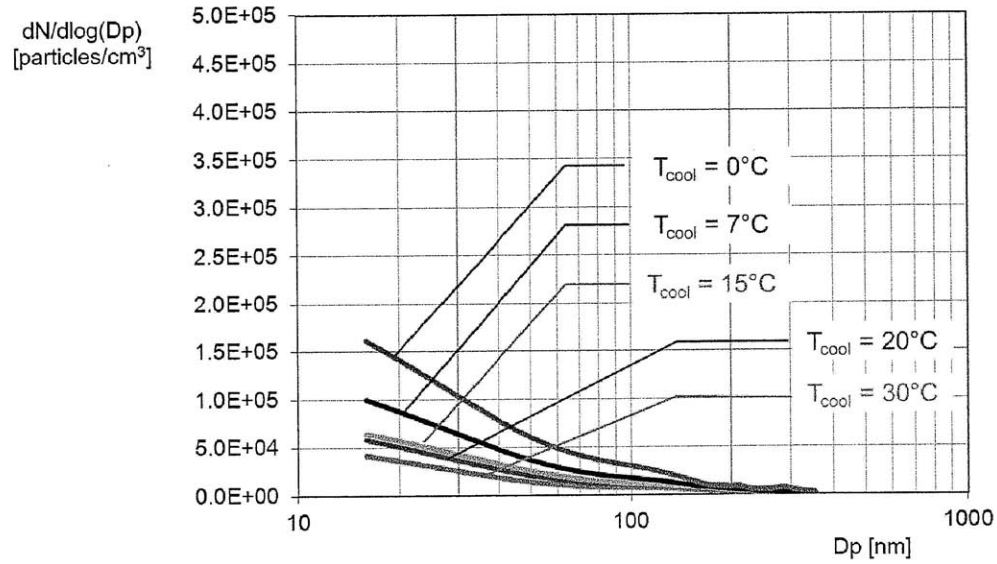

Figure 3.5. *The PN distribution under cold-start conditions for* ***E85*** *(85% by vol. ethanol. and 15% by vol. gasoline).*

From the PN distributions for the tested gasohol blends, presented above, we can observe the following:

1. The shape of the distribution is the same for all tests. This emphasizes that the shape of

the PN distribution is a function of engine operating conditions.

2. The presence of only 10% by volume ethanol in the fuel blend suppressed the PM formation for all temperatures. However, the increase of ethanol content from 10% to 85% did not have any additional effect on PM emissions. To explain this, we should consider two factors that are the disadvantages of ethanol compared to gasoline: ethanol's higher heat of evaporation and ethanol's lower heating value. This means that although the increase of ethanol content may reduce the aromatics in the fuel (thus less potential for PM formation), for the same output, we have to inject more fuel, which will need more time to evaporate. The later increases the probability of fuel impinging the cylinder walls, thus increasing the PM emissions.

A final conclusion from plotting the PN distributions for all fuels at 30°C and at 7°C is that at lower engine temperatures, the reduction PM mechanism due to ethanol presence is more effective than at higher engine temperatures 3.6).

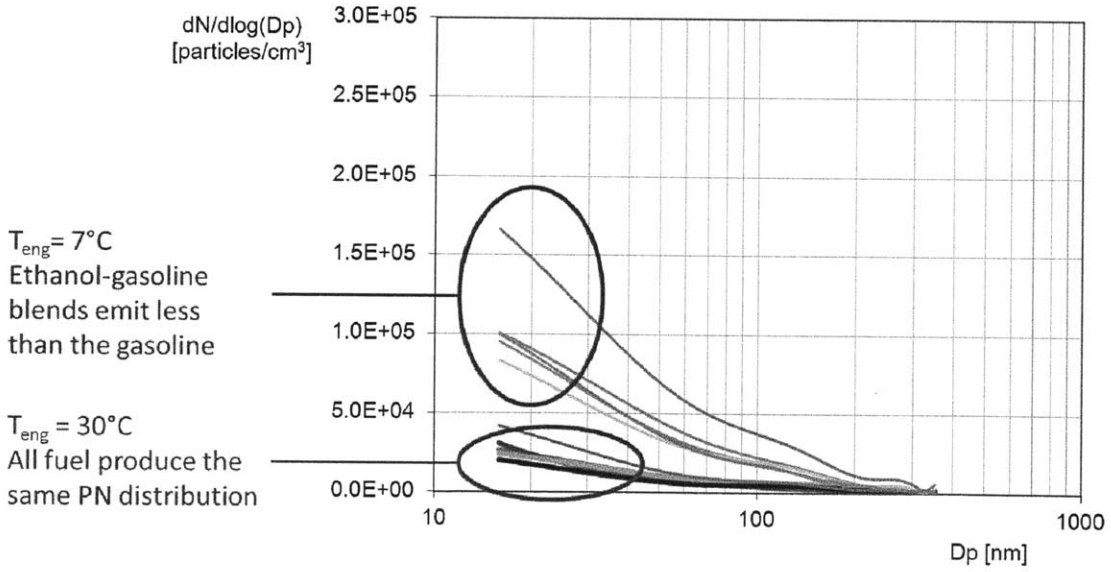

Figure 3.6. *The effect of ethanol presence in the fuel on PN distribution at 30° C and at 7° C.*

3.2 The effect of ethanol on PM formation

The PN distributions are similar for all tested fuels. The particles with an electrical equivalent diameter less than 150 nm, are orders of magnitude higher than the rest. Thus, instead of presenting the same graphs as Figures 3.1 - 3.5 by simply rearranging them (plot all fuels at each temperature), we calculate the total emitted PN and we plot them as a function of the engine's temperature for all tested fuels (Figure 3.7). The total PNs have been calculated by integrating the PN distributions for each case (Formula 1.3).

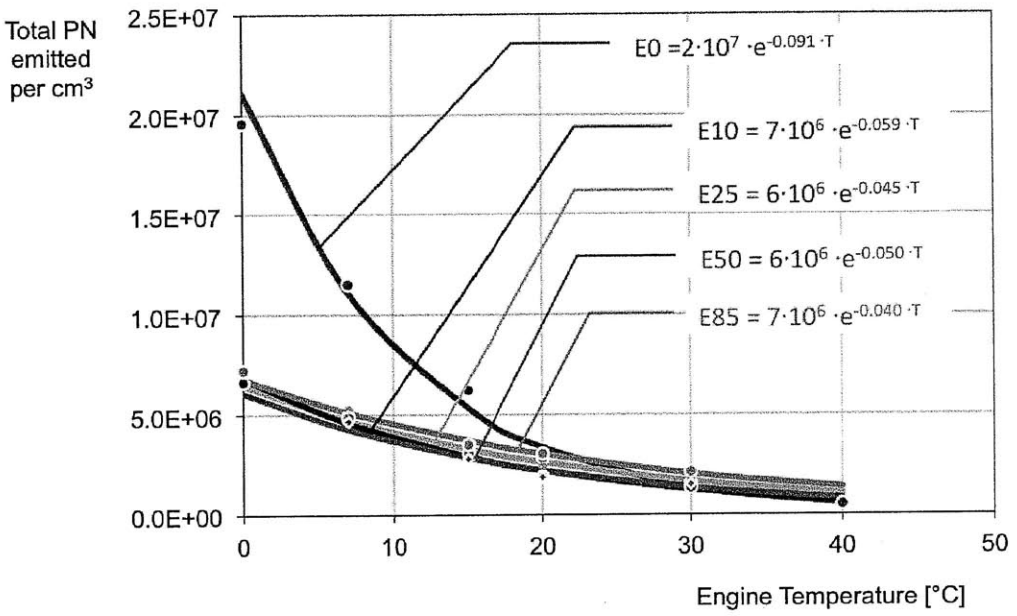

Figure 3.7. *For temperatures less than 20° C, gasoline (E0) emits an order of magnitude higher PN than the gasohol blends. For all gasohol blends with ethanol content in the fuel 10% or more, the emitted PN are the same for all engine temperatures.*

From Figure 3.7 we can draw the following observations:

1. For the engine conditions used during these experiments, the total PN emissions for all fuels fit well to exponential functions of engine temperature (i.e., $f(T) = a \cdot e^{b \cdot T}$, where a and b are constants).

2. For engine temperatures less than 20°C, gasoline emits an order of magnitude higher PN than the gasoline-ethanol blends.

3. For engine temperatures higher than 20°C, all tested fuel emit the same total PN.

4. For all temperatures, all tested gasoline-ethanol blends emit the same total PN.

A possible reason for observations two and three is the following two phenomena: a) in general, gasoline evaporates faster that ethanol; b) in order to achieve the same engine power output at the same operating conditions, we need to inject more fuel as ethanol content increases (Figure 3.8). The combination of these phenomena has the following effects: the increase of ethanol in the gasohol blends decreases the aromatic content of the fuel (thus less potential for PM formation), but at the same time more fuel mass is injected, which is more difficult to evaporate (thus higher probability for PM formation due to fuel impinging the cylinder walls and the piston).

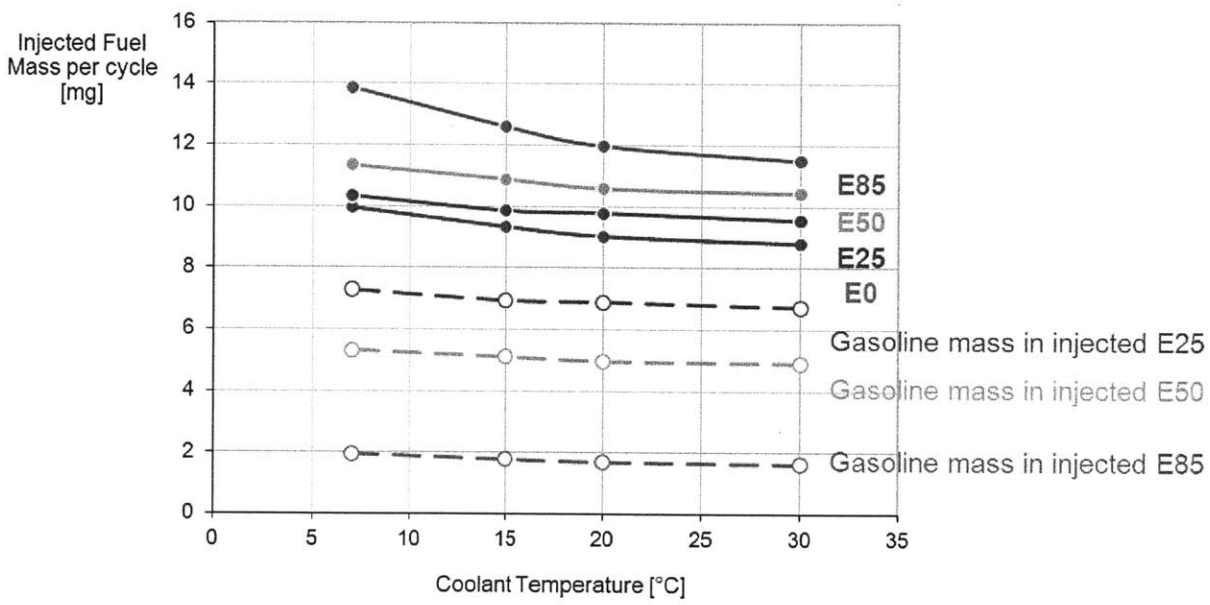

Figure 3.8. *The injected fuel mass for E0, E25, E50 and E85, for a temperature range between 7 and 30° C. The increase of ethanol content in the fuel decrease the gasoline content of the fuel (doted lines), thus the aromatics; however for the same engine output the total fuel mass of the gasohol blends is higher (straight lines) than E0 and harder to evaporate.*

Although it has not been confirmed experimentally, a possible explanation for observation four comes from the soot yield of gasoline-ethanol blends. Previous research, for fuels tested in a rapid compression machine (RCM), shows that for fuel-air equivalence ratios (ϕ) below a critical range, the soot yield for mixture of n-butane, Ar and O_2 reduces significantly (Figure 3.9). Although curves similar to the one in Figure 3.9 have not been produced for the tested ethanol-gasoline blends, the presence of 10% ethanol in the fuel may be enough to reduce the ϕ of the locally rich areas in the combustion chamber below that critical limit. As a result,

the soot yield of the E10 decreases significantly. The increase of ethanol in the fuel (E25, E50, E85) will reduce the ϕ even more. However, since ϕ is already below the critical value, the extra amount of ethanol does not make a significant difference in the PM formation any more.

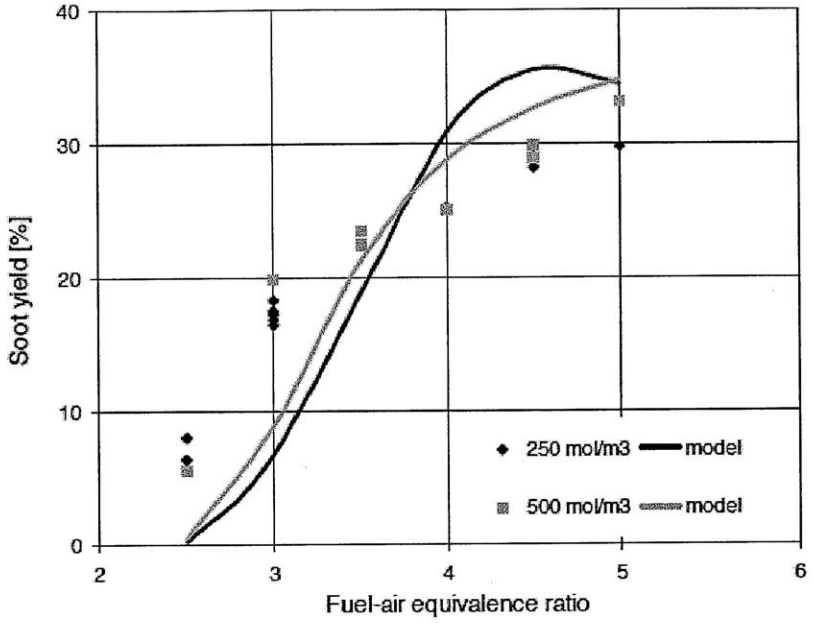

Figure 3.9. *Soot yield experimental data and modeling results of n-butane/Ar/O_2 mixtures (Ar/O_2=3.773) for T=770°K [13]. For $\phi < 3$ the soot yield is three times less than $\phi > 4$.*

From the data in Figure 3.7, we see a "jump" on the emitted PN from E0 to E10. In order to evaluate the actual fuel composition where the transition occurs we run two more fuels: E2.5 (2.5% ethanol-97.5% gasoline) and E5 (5% ethanol-95% gasoline). Figure 3.10 shows the results for the four fuels.

E2.5 and E5 have the same behavior as the rest of the fuels for engine temperatures higher than 20°C. For lower temperatures E2.5 emits slightly less PN than E0, and E5 emits, on average, half of the PN emitted from E0 for the same temperatures. Thus, there is a transition from E0 to E10, as far as the PN is concern, but after E10 no significant difference on PN due to higher ethanol content has been recorded.

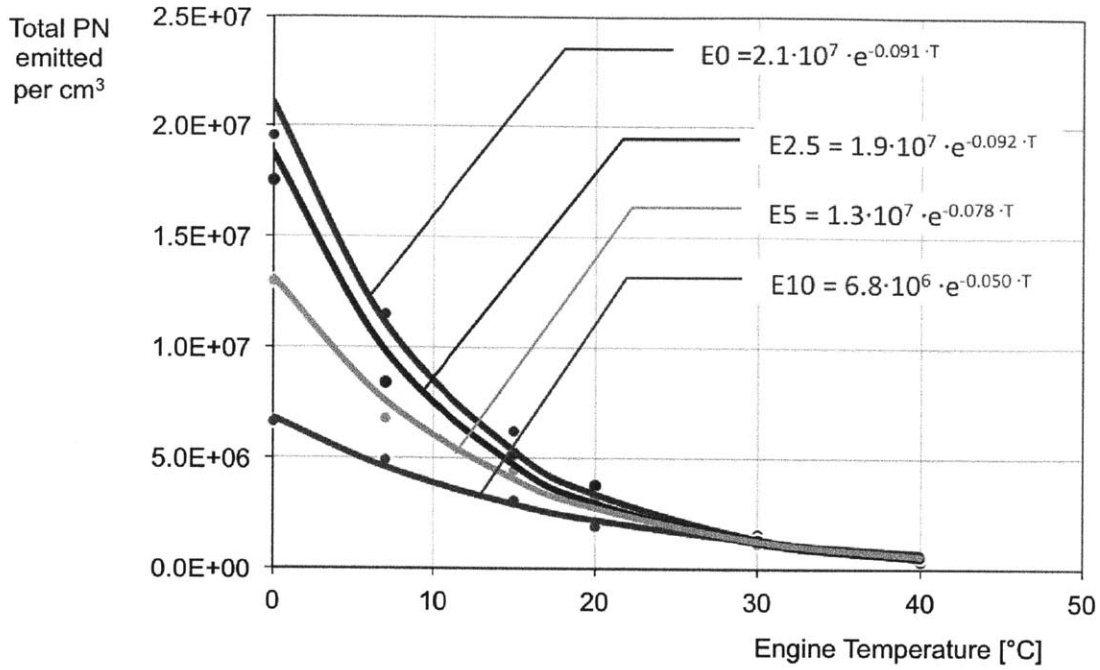

Figure 3.10. *By running E5 and E2.5 we can see the transition in PN emission increase from E10 to E0.*

3.3 Conclusions

The introduction of DISI engine improved the overall efficiency of the gasoline engines and made it the primary choice for light duty vehicles. However, DISI engines still suffer from high PM emissions. Due to the relation of several diseases with the size of PM, emitted from internal combustion engines, nowadays governments globally impose stricter legislations for PM emissions from ICEs. Given that the majority of PM is emitted during the first few minutes of engine operation (cold-start), a proposed PM reduction strategy has been investigated: the introduction of ethanol content in the fuel. In order to measure the effects of ethanol-gasoline fuel blends on PN emissions at a range of engine temperatures during cold-start conditions, a mini-dilution tunnel, coupled with an SMPS system, has been used. The focus of this research is on engine-out emissions, so that samples are collected at a short distance (15 cm) from the exhaust valves.

From the results of the work, we can summarize the following conclusions:

1. A monotonic PN distribution with values decreasing with increase of particle size is observed for all the fuels and at all the engine coolant temperatures (ECTs) tested. The local peak (identified as due to particle agglomeration) which has been observed in tailpipe sampling is not observed.

2. For gasoline (E0), the PN values for D_p less than 100 nm increase with decrease in ECT. The change is modest for ECT change from 40°C to 20°C. The increase, however, is substantially larger when ECT is lower than 15°C. This observation is attributed to the non-linear dependence of evaporation to temperature.

3. For E10 to E85, the shape of the PN distribution is similar to that derived from E0. However, there is only a modest increase in the PN values, when ECT is changed from 30°C to 0°C. Furthermore, both the shape and values of the distribution at the same ECT are insensitive to the alcohol content in the fuel. Thus at low ECT, there is a sharp drop of PN from E0 to E10, but further increase in ethanol content does not produce any further PN changes.

4. At ECT above 20°C, the total PN (integrated over the distribution from 15 to 350 nm) is insensitive to the fuel ethanol content.

5. At ECT $<$ 20°C, the total PNs for E10 to E85 are almost identical, and the values increase modestly with decrease of ECT. For E0, however, the PN values are substantially higher; e.g. at 0°C ECT, the total PN emission from E0 is more than 3 times that from E10. Thus there is a substantial change in PN emissions when the fuel is changed from E0 to E10, and very little change is observed with further increase in ethanol content from E10 to E85.

6. The above observation is confirmed by emissions measurements with E2.5 and E5. The midpoint of the change in total PN value from E0 to E10 occurs approximately at E5.

7. Because the evaporative property of the fuel does not change significantly from E0 to E10, the substantial reduction in PN with ethanol is attributed to the effect of ethanol on PM chemistry.

3.4 Future work

The PM formation mechanisms in internal combustion engines are a series of complicated chemical and physical phenomena. The parameters that influence the PM formation are not easy to isolate in an engine environment; at the same time, a lot of the end result comes from combinations of these phenomena in the combustion chamber.

For example, this set of experiments does not investigate fully the effect of the intake air temperature on PN formation. Although this is part of the next step of this research project, we verify that the number of PM emissions depend on the intake air temperature as well. By repeating the experiment in spring and in summer (air intake temperature difference of 10°C), we quantify this effect and check that the PN distributions can be compared, when taken at the same air intake temperature. Figures 3.11, 3.12 and 3.13, show the difference of the PN distributions, during cold start conditions, for E0 at engine temperatures of 20, 15 and 7°C, in spring and in summer.

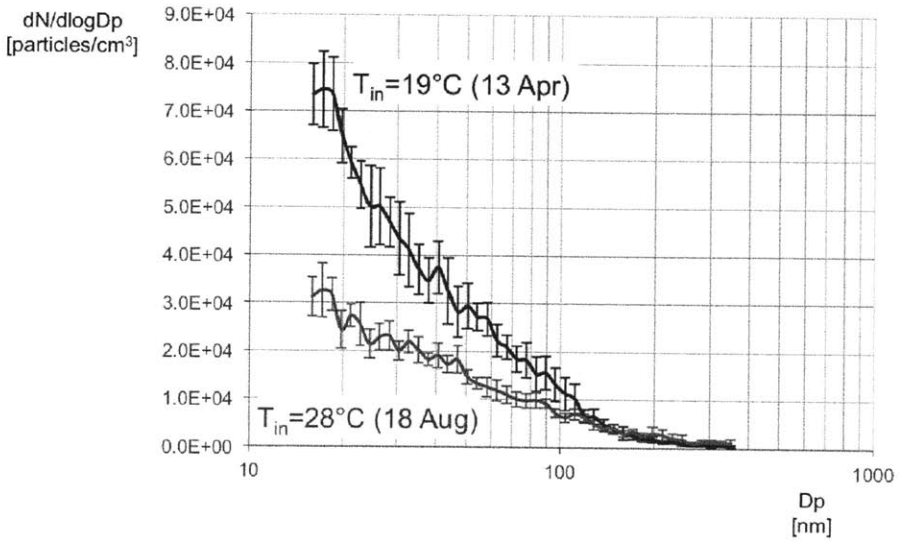

Figure 3.11. *PN distributions for E0 at* ***engine temperature of 20° C****, under cold start conditions for intake air temperatures of 19 and 28° C. Hotter intake air decreases the number of PM, especially for nano-particles(diameter<100 nm). The line represent the average of ten PN distributions and the error bars show the 90% confidence interval.*

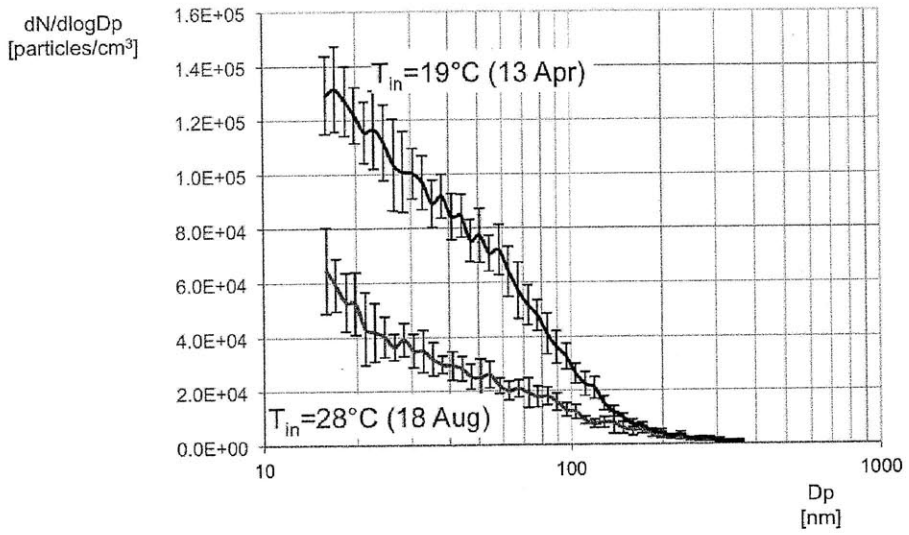

Figure 3.12. *PN distributions for E0 and* ***engine temperature at 15° C****, under cold start conditions for intake air temperatures of 19 and 28° C. The effect on PN is similar with the previous FIgure.*

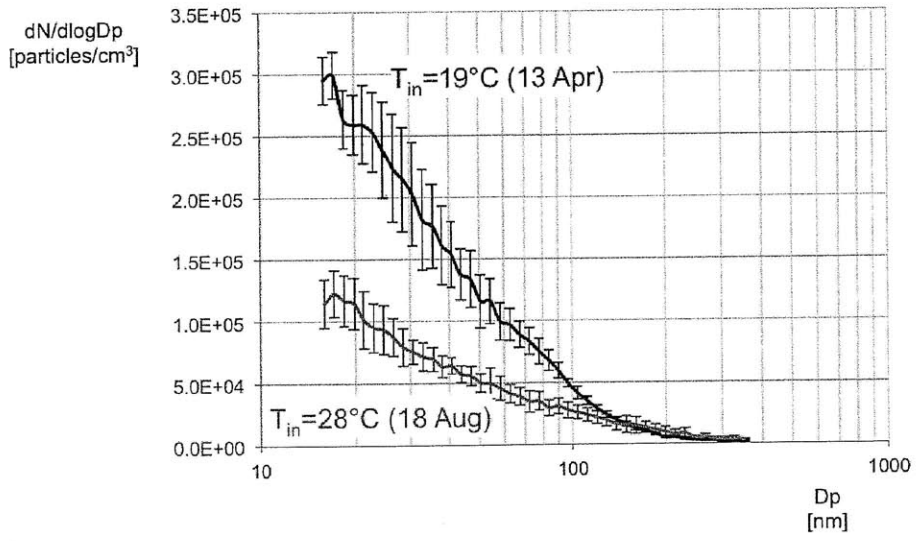

Figure 3.13. *PN distributions for E0 and* ***engine temperature at 7° C****, under cold start conditions for intake air temperatures of 19 and 28° C. The effect on PN is similar with the previous two Figures.*

From these figures we conclude that the lower the intake air temperature, the higher the PN. Although this will change the absolute number of the emitted PN, it is more important to verify that the intake air temperature will not change the PM formation mechanisms. Figures 3.14 and 3.15 show the PN distributions for two engine temperature decrease steps, one from 20 to 15°C and one from 15 to 7°C . For both intake air temperatures the average increase of emitted PN, for sizes between 15 and 100 nm, is the same for both engine temperature decrease steps. From these data, we can conclude that the air intake temperature can vary the absolute number of emitted PM, but it does not change the PM formation mechanism. The data presented in the previous sections are for under the same air intake temperature.

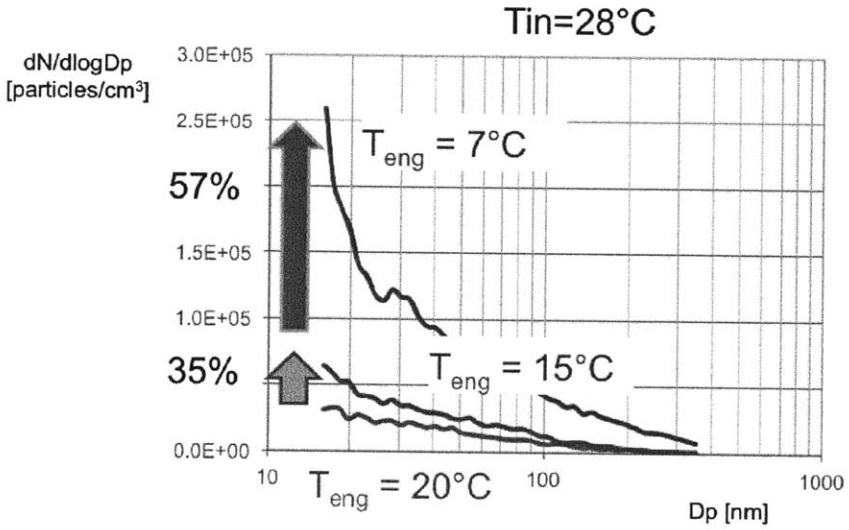

Figure 3.14. *For intake air temperature of 28° C, decreasing the engine temperature from 20 to 15° C results to an average increase of PN, with sizes between 15 and 100 nm, of 35%. For even more reduction of engine temperature from 15 to 7° C the average increase in PN is 57%.*

From the example presented above, it is obvious that this work has not covered every aspect of the problem. As previous stated, differentiating between the mechanisms that lead to PM formation is challenging. Some new steps that could be taken are the following: a) a series of RCM tests can be conducted in order to verify (or disprove) the hypothesis of the critical value of ϕ in soot yield for the tested ethanol-gasoline blends; b) by sampling exhaust gases on a filter paper and conducting further analysis (such as TGA) of the sample, the chemical components of the exhaust for the different conditions can be evaluated; c) also, exhaust gases can be sampled on a small copper grid surface and analyzed under a TEM microscope to compare the structure formation of the PM at each case. These are some of the next steps in order to frame the ethanol effect on PM formation.

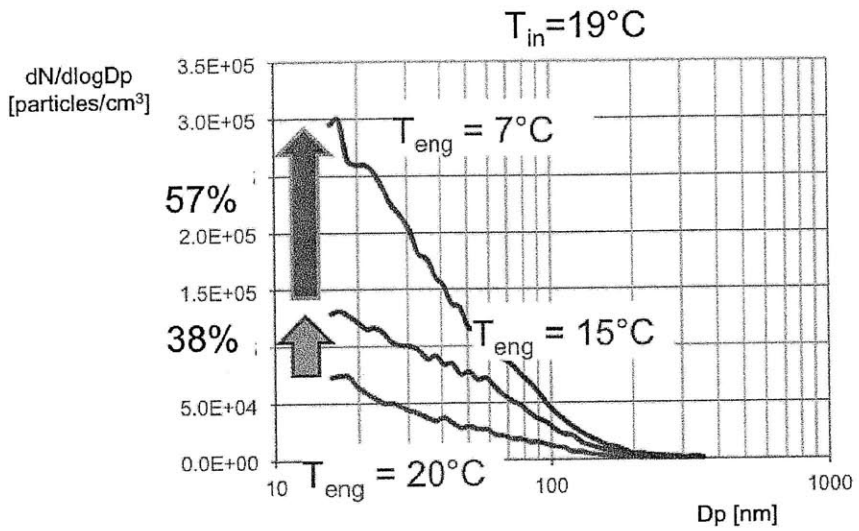

Figure 3.15. *Hotter intake air decreases the number of PM, especially for particle sizes with electrical equivalent mobility diameter less than 120 nm. The line is the average and the error bars show the 90% confidence interval from ten PN distributions.*

In combination with the experimental aspect of this study, a modeling approach using Computational Fluid Dynamics software can be beneficial. This modeling can be used to draw further conclusions related to fuel impinging the cylinder walls and the piston heads, and the evaporation process for each of the ethanol-gasoline blends.

Finally, there are other in-cylinder strategies that may prove to be more cost-effective controlling the emitted PM from DISI engines (including the use of advanced fuel injectors and optimization of engine calibration, such as ignition and injection timing, split injection, fuel injection pressure), and at the same time, minimizing any trade-offs with other emissions, fuel efficiency (CO_2) and engine durability. In any case, it would be beneficial to conduct a new series of experiments in a 2nd generation DISI engine (spray guided).

Today, it is more critical then ever to focus our research efforts on developing strategies to reduce emissions from internal combustion engines. People pollute the atmosphere and compromise their health because they are not willing to sacrifice their conveniences. Let's hope that, over the next years, the main design parameter for new engines will be their ability to emit less pollutants.

Appendix A

Procedure to adjust SMPS flow rates for the model 3010 CPC

1. Fill the table in Figure A.2 according to the desired flow rates (using the SMPS operating range vs flowrate table - Figure A.1):

SMPS Operating Range vs. Flowrate, Impactor ΔP, and 50% Cut Size vs. Flowrate

Polydisperse Aerosol Flowrate (lpm)	0.0457 cm Orifice		0.0508 cm Orifice		SMPS Range (nm)	Impactor to Use
	ΔP* (cm H_2O)	50% Cut (μm)	ΔP* (cm H_2O)	50% Cut (μm)		
0.2	2.50	0.846	1.90	1.006	16–1000	0.0508
0.25	3.94	0.748	2.56	0.892	15–960	0.0508
0.3	5.66	0.677	3.71	0.808	13–835	0.0508
0.4	10.1	0.576	6.58	0.6900	12–670	0.0457
0.5	15.8	0.508	10.3	0.6090	10–560	0.0457
0.6	22.7	0.457	14.8	0.5500	10–485	0.0457
0.7	30.9	0.418	20.1	0.5030	9–435	0.0457
1.0	61.2	0.338	40.0	0.4090	7–325	0.0457
2.0	—	—	—	—	5–200	none

*Actual pressure drop is usually greater than predicted due to surface roughness and imperfections in the nozzle.

Figure A.1. *SMPS Operating Range vs. Flowrate, Impactor ΔP, and 50% cut size vs. Flowrate.*

2. Before tuning the vacuum pump:

a. Open sheath air valve (fully open)

b. Close monodisperse aerosol valve (fully closed)

c. Open excess air valve (fully open, do not adjust)

Flowmeter Set Points

Parameter	Monodisperse Air	Sheath Air	Excess Air
Flowrate (lpm.)			
Output (volts)			
Pressure (Cm. H_2O)			

Figure A.2. *Flowmeter Set Points*

d .Close external valve subassembly (fully closed)

3. Turn on the CPC.

4. Turn on the Electrostatic Classifier.

5. Apply power to vacuum pump.

After a while all the LEDs should light. The LIQUID LED may or may not light, but the CPC could be operate, provided there is fluid visible in the LIQUID LEVEL WINDOW.

6. Slowly open/adjust the external valve subassembly until the desires flow rate is reached on the excess air flowmeter.

7. Slowly open/adjust the monodisperse aerosol valve for the proper voltage reading (depending on the desired flowrate).

8. Readjust the excess air flow (repeat step 5).

9. Slowly open/adjust the sheath air valve to the proper flow rate, checking the pressure gauge for the correct pressure drop.

10. Fine adjustments to the desired voltage values:
a. First adjust the excess air flowrate using the meter selector (right) knob on the classifier.
b. Then adjust the monodisperse aerosol flowrate using the meter selector (left) knob.
c. Finally adjust the sheath air flowrate by checking the pressure gauge for the correct pressure.
If the sheath air reading is not within 20 [mV] of the value given in the above table:

a. Check the fittings to ensure they are leak-tight

b. Check the plumbing configuration

c. Compare the sheath air to the excess air voltages to ensure they match the charted values. If the match, the flow rates should be equal.

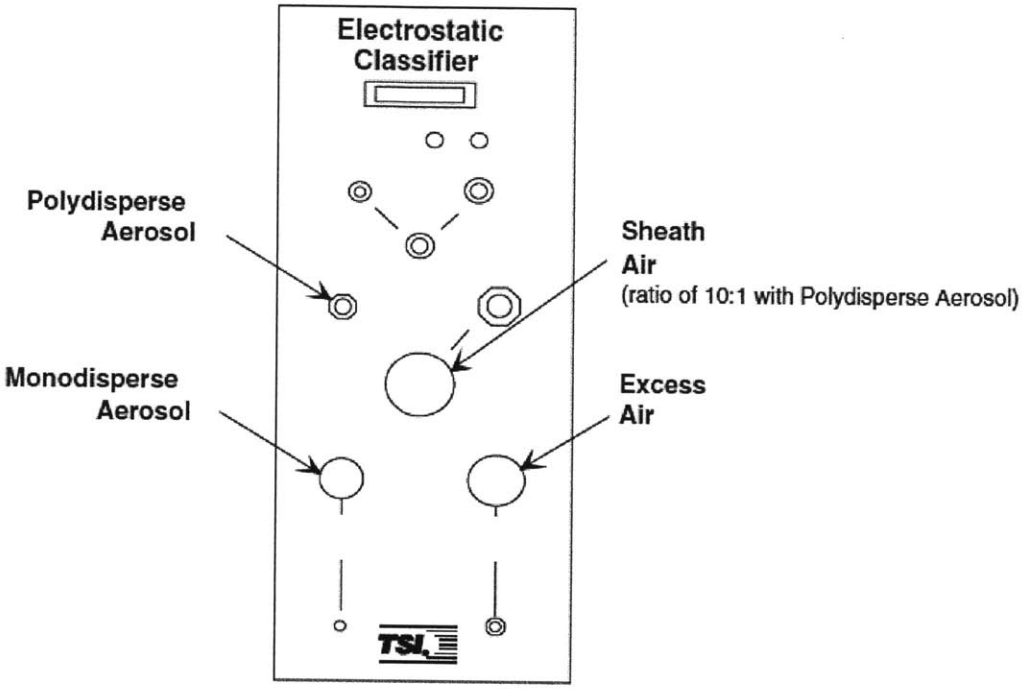

Figure A.3. *All flows can be adjusted via the knobs on the Electrostatic Classifier unit.*
Adjusting the flowrates:
a. Sheath air flowrate : Polydisperse aerosol flowrate = 10 : 1
b. Sheath air flowrate = Excess air flowrate
c. Polydisperse aerosol flowrate = Monodisperse aerosol flow.

Appendix B

Gasoline Fuel Specifications: Haltermann HF0437

PRODUCT INFORMATION

Haltermann
PRODUCTS

T (800) 969-2542 F (281) 457-1469

RESPONSIBLE CARE
ISO 9001 CERTIFIED

Johann Haltermann Ltd.

PRODUCT: EPA TIER II EEE
FEDERAL REGISTER

PRODUCT CODE: HF437

Batch No.: XE1421LT10
Shipment No: MTS
Tank No.: 107
Analysis Date: 5/15/2009

TEST	METHOD	UNITS	FED Specs		HALTERMANN Specs			RESULTS
			MIN	MAX	MIN	TARGET	MAX	
Distillation - IBP	ASTM D86	°F	75	95	75		95	87
5%		°F						108
10%		°F	120	135	120		135	123
20%		°F						145
30%		°F						170
40%		°F						201
50%		°F	200	230	200		230	223
60%		°F						235
70%		°F						248
80%		°F						270
90%		°F	305	325	305		325	319
95%		°F						333
Distillation - EP		°F		415			415	386
Recovery		vol %				Report		97.0
Residue		vol %				Report		1.0
Loss		vol %				Report		2.0
Gravity	ASTM D4052	°API			58.7		61.2	59.4
Density	ASTM D4052	kg/l			0.734		0.744	0.741
Reid Vapor Pressure	ASTM D5191	psi	8.7	9.2	8.7		9.2	9.0
Carbon	ASTM D3343	wt fraction				Report		0.0000
Carbon	ASTM E191	wt fraction				Report		0.8649
Hydrogen	ASTM E191	wt fraction				Report		0.1326
Hydrogen/Carbon ratio	ASTM E191	mole/mole				Report		1.826
Stoichiometric Air/Fuel Ratio						Report		14.549
Oxygen	ASTM D4815	wt %					0.05	<0.01
Sulfur	ASTM D5453	wt %	0.0015	0.0080	0.0025		0.0035	0.0028
Lead	ASTM D3237	g/gal		0.05			0.01	<0.01
Phosphorous	ASTM D3231	g/gal		0.005			0.005	<0.0001
Silicon	ASTM 5184	mg/kg					4	<1
Composition, aromatics	ASTM D1319	vol %		35.0			35.0	27.1
Composition, olefins	ASTM D1319	vol %		10.0			10.0	0.6
Composition, saturates	ASTM D1319	vol %				Report		72.3
Particulate matter	ASTM D5452	mg/l					1	0.8
Oxidation Stability	ASTM D525	minutes			240			>1000
Copper Corrosion	ASTM D130						1	1a
Gum content, washed	ASTM D381	mg/100mls					5	1
Fuel Economy Numerator/C Density	ASTM E191				2401		2441	2428
C Factor	ASTM E191					Report		1.0033
Research Octane Number	ASTM D2699		93.0		96.0			97.4
Motor Octane Number	ASTM D2700					Report		89
Sensitivity			7.5		7.5			8.3
Net Heating Value, btu/lb	ASTM D3338	btu/lb				Report		18502
Net Heating Value, btu/lb	ASTM D240	btu/lb				Report		18404
Color	VISUAL					Report		Undyed

APPROVED BY:

ANALYST PLI/PH/DIX/GP

Bibliography

[1] Al. Alkidas and Sh. Tahry, *Contributors to the Fuel Economy Advantage of DISI Engines over PFI Engines*, SAE Technical Paper 2003-01-3101 (2003).

[2] Alex Alkidas, *Combustion Advandages in Gasoline Engines*, Energy Conversion and Management **48** (2007), 2751–2761.

[3] R.W. Anderson, J. Yang, D.D. Brehob, J.K. Vallance, and Whiteaker R.M., *Understanding the Thermodynamics of Direct-Injection Spark-Ignition Combustion Systems: an Analytical and Experimental Investigation*, SAE Technical Paper 962018 (1996).

[4] California Air Resources Board, *Estimate of premature deaths associated with fine particle pollution (pm2.5) in california using epa's methodology*, California Environmental Protection Agency, 2010.

[5] Mike Braisher, Richard Stone, and Phil Price, *Particle Number Emissions from a Range of European Vehicles*, SAE Technical Paper 2010-01-0786 (2010).

[6] W.K. Cheng, D. Hamrin, J.B. Heywood, S. Hochgreb, K.D. Min, and M. Norris, *An overview of hydrocarbon emissions mechanisms in spark-ignition engines*, SAE Technical Paper 932708 (1993).

[7] R.L. Cole, R.B. Poola, and R. Sekar, *Exhaust Emissions of a Vehicle with a Gasoline Direct-Injection Engine*, SAE Technical Paper 982605 (1998).

[8] Peter Eastwood, *Particulate Emissions from Vehicles*, John Wiley & Sons, Ltd, West Sussex, England, 2008.

[9] Sheldon Friedlander, *Smoke, Dust and Haze: Fundamentals of Aerosol Dynamics, Second Edition*, Oxford University Press, Inc, New York, NY, 2008.

[10] José Geiger, Michael Grigo, Oliver Lang, Peter Wolters, and Patrick Hupperich, *Direct Injection Gasoline Engines - Combustion and Design*, SAE Technical Paper 1999-01-0170 (1999).

[11] William Hinds, *Aerosol Technology: Properties, Behavior and Measurement of Airborne Particles, Second Edition*, John Wiley & Sons, Inc, New York, NY, 1999.

[12] Y. Iwamoto, K. Noma, O. Nakayama, T. Yamauchi, and H. Ando, *Development of Gasoline Direct Injection Engine*, SAE Technical Paper 970541 (1997).

[13] Ioannis Kitsopanidis, *PhD Thesis: Experimental and Computational Study of Soot Formation under Diesel Engine Conditions*, Massachusetts Institute of Technology, 2004.

[14] Hyungmin Lee, Cha-Lee Myung, and Simsoo Park, *Time-resolved particle emission and size distribution characteristics during dynamic engine operation conditions with ethanol-blended fuels*, Fuel **88**, 1680–1686.

[15] Z.A. Mansurov, *Soot Formation in Combustion Processes (Review)*, Combustion, Explosion and Shock Waves **41**, no. 6.

[16] Arden Pope III, Richard Burnett, Michael Thun, Eugenia Calle, Krewski Daniel, Kazuhiko Ito, and George Thruston, *Lung Cancer, Cardiopulmonary Mortality, and Long-term Exposure to Fine Particulate Air Pollution*, The Journal of the Amierican Medical Association (2002).

[17] C. Preussner, C. Doering, S. Fehler, and S. Kampmann, *GDI: Interaction Between Mixture Preparation, Combustion System and Injector Performance*, SAE Technical Paper 980498 (1998).

[18] P. Price, R. Stone, T. Collier, and M. Davies, *Particulate Matter and Hydrocarbon Emissions Measurements:Comparing First and Second Generation DISI with PFI in Single Cylinder Optical Engines*, SAE Technical Paper 2006-01-1263 (2006).

[19] Philip Price, Richard Stone, Dave OudeNijeweme, and Xiangdong Chen, *Cold Start Particulate Emissions from a Second Generation DI Gasoline Engine*, SAE Technical Paper 2007-01-1931 (2007).

[20] Phillip Price, *PhD Thesis: Direct Injection Gasoline Engine Particulate Emissions*, University of Oxford, 2009.

[21] Michael Radovanovic, *Hydrocarbon Emissions in a Homogeneous Direct Injection Spark Ignited Engine*, MIT, MSc Thesis, Cambridge, MA, 2006.

[22] U. Spicher, J. Reissing, J. Kech, and J. Gindele, *Gasoline Direct Injection Engines Development Potentialities*, SAE Technical Paper 1999-01-2938 (1999).

[23] C. Stan, *Direct Injection Systems: The next decade in Engine Technology*, Society of Automotive Engineers, Warrendale, PA, 2002.

[24] G. Szekely and Al. Alkidas, *Combustion Characteristics of a Spray-Guided Direct-Injection Stratified-Charge Engine with a High-Squish Piston*, SAE Technical Paper 2005-01-1937 (2005).

[25] Fuquan Zhao, David Harrington, and Ming-Chia Lai, *Automotive Gasoline Direct-Injection Engines*, Society of Automotive Engineers, Inc., Warrendale, PA, 2002.